JOURNAL OF CLINICAL IMMUNOLOGY AND MICROBIOLOGY

E-ISSN: 3068-5168
Journal of Clinical Immunology & Microbiology

ATHENAEUM SCIENTIFIC PUBLISHERS

Research Article

Regulation of IgE-Mediated Allergic Reactions by Disulfide-Linked Multimers of Histamine-Releasing Factor

Yu Kawakami[1,13], Tomoaki Ando[2,3,5], Ryoji Ito[6], Kazumi Kasakura[1,13], Risa Yamamoto[1,13], Sung-Wook Hong[7,13], Giuseppe Destito[8], Julienne Ferrer[1], John Laudenslager[8,13], Kacey Sachen[8,13], Simon Belanger[9,13], Kyoichi Isono[4,13], Jun-ichi Kashiwakura[2,13], Scott A. Smith[10], Charles D. Surh[7,14], Hiromi Kubagawa[11], Toshiaki Maruyama[12], Yuko Kawakami[1], Toshiaki Kawakami[1,2*]

[1]Laboratory of Allergic Diseases, Center for Autoimmunity and Inflammation and [9]Center for Infectious Disease and Vaccine Research, La Jolla Institute for Immunology, La Jolla, California 92037, USA

[2]Laboratory for Allergic Disease, [3]Laboratory for Cytokine Regulation, and[4]Laboratory for Developmental Genetics, RIKEN Center for Integrative Medical Sciences, Yokohama 230-0045, Japan

[5]Atopy Research Center, Graduate School of Medicine, Juntendo University, Tokyo 113-8421, Japan

[6]Central Institute for Experimental Animals (CIEA), Kawasaki 210-0821, Japan

[7]Academy of Immunology and Microbiology, Institute for Basic Science, Pohang, Republic of Korea and Department of Integrative Biosciences and Biotechnology, Pohang University of Science and Technology, Pohang, Republic of Korea

[8]Kyowa Kirin, Inc., La Jolla, California 92037, USA;

[10]Department of Pathology, Microbiology and Immunology, Vanderbilt University, Nashville, Tennessee 37232, USA

[11]Humoral Immune Regulation, Deutsches Rheuma-Forschungszentrum (DRFZ), Berlin, Germany

[12]Abwiz Bio, San Diego, California, USA

[13]Current Address: (Yu K.) Kyowa Kirin, Inc., La Jolla, California 92037, USA; (S.-W.H.) Yonsei University, Seoul, Republic of Korea; (R.Y.) Faculty of Medicine, Juntendo University, Tokyo, Japan; (K.K.) Janssen Pharmaceutical K.K., Tokyo, Japan; (J.L.) Janux Therapeutics, San Diego, California 92130, USA; (K.S.) The Janssen Pharmaceutical Companies of Johnson & Johnson, San Diego, California 92121, USA; (S.B.) VIR Biotechnology, Inc., San Francisco, California 94158, USA; (K.I.) Laboratory Animal Center, Wakayama Medical University, Wakayama, Japan; (J.K.) Hokkaido University of Science, Sapporo, Japan

[14]Deceased on October 7, 2017

***Correspondence author:** Toshiaki Kawakami, MD, PhD. La Jolla Institute for Immunology, 9420 Athena Circle, La Jolla, California 92037, USA;
Email: toshi@lji.org

Citation: Kawakami Y, et al. Regulation of IgE-Mediated Allergic Reactions by Disulfide-Linked Multimers of Histamine-Releasing Factor. J Clin Immunol Microbiol. 2026;7(1):1-29.

https://doi.org/10.46889/JCIM.2026.7107

Received Date: 26-02-2026

Accepted Date: 15-03-2026

Published Date: 23-03-2026

Abstract

Background: Stimulation with allergen and allergen-specific IgE activates mast cells, leading to allergic reactions. We studied how the recently defined alarmin, Histamine-Releasing Factor (HRF), promotes this immune response.

Methods: HRF reactivity to IgE and other Ab isotypes was analyzed by *in-vitro* binding assays and 3D-structure modelling. Extracellular and intracellular formations of HRF multimers were studied in aqueous solution and siRNA-treated cells, respectively. Effects of HRF dimers and multimers on *in-vitro* mast cell activation were measured in IgE-sensitized mast cells by stimulation with high or low valency antigen. *In-vivo* effects of HRF in allergic reactions were studied in passive anaphylaxis and food allergy models using WT or non-multimerizable HRF mutant mice as well as humanized mice.

Results: HRF binds to a substantial subset of both antigen-driven and non-antigen-driven antibodies. Extracellular HRF proteins become non-enzymatically disulfide-linked dimers and multimers, whereas intracellular HRF requires oxidoreductases for dimerization. Surprisingly, while HRF dimers can enhance antigen/IgE-induced cytokine production, stronger signals by HRF multimers are required for degranulation. HRF multimers render HRF-reactive IgE-sensitized mast cells more sensitive and responsive to suboptimal antigen doses. *In-vivo* anaphylactic responses induced by passive sensitization with HRF-reactive IgE and subsequent antigen challenge are drastically reduced by blockade of HRF-IgE interactions and by HRF-Cys172Ala mutation in mutant mice. Enhancement of anaphylactic responses by HRF is more prominent with low-valency antigen than with supernaturally high-valency antigen.

Conclusion: The results collectively demonstrate that HRF multimers are important for IgE-mediated optimal allergic reactions.

Keywords: Allergy; Mast Cell; IgE; FcεRI; Histamine-Releasing Factor

Abbreviation

FcεRI: High-Affinity Ige Receptor; DNP: Dinitrophenyl; TNP: Trinitrophenyl; GF: Germ-Free; HRF: Histamine-Releasing Factor; TCTP: Translationally Controlled Tumor Protein; HDM: House Dust Mite; SPF: Specific Pathogen-Free; EBV: Epstein-Barr Virus; mHRF: Mouse HRF; SHM: Somatic Hypermutation; hHRF: Human HRF; siRNA: Short-Interfering RNA; BMMCs: Bone Marrow-Derived Mast Cells; AMBER: Assisted Model Building With Energy Refinement; BSA: Buried Surface Area; ΔiG: Solvation Free Energy Gain; PSA: Passive Systemic Anaphylaxis; PCA: Passive Cutaneous Anaphylaxis; OVA: Ovalbumin; NP: 4-Hydroxy-3-Nitrophenylacetyl

Introduction

Allergic reactions induced by exposure to allergen follow a course of the acute and often late and chronic reactions [1]. The acute-phase reaction is caused by degranulation of mast cells, which releases the preformed contents of secretory granules including histamine, serotonin and proteases, while late-phase reactions seen hours after allergen exposure are caused by preformed and de novo synthesized allergic mediators such as TNF and other cytokines secreted from activated mast cells. Chronic reactions occurring days later are due to basophil activation [1].

Allergic reactions are characterized by exquisite sensitivity to a minute amount of antigen and a great magnitude of rapid reactions. Binding of multivalent antigen to IgE molecules, which have bound to high-affinity IgE receptors (FcεRI) on the mast cell surface, crosslinks IgE-FcεRI complexes, triggering activation signals within the cells [2,3]. Four types of antigen are assumed for IgE-bound FcεRI crosslinking: A) a single antigen with multiple identical epitopes, B) an oligomeric antigen with an identical epitope in the monomer, C) a single antigen with two or more different epitopes and D) a combination of two or more antigens (e.g., B and C) [4]. Consistent with this notion, the minimal antigen valency of 2 is required for IgE-dependent mast cell activation [5]. Most mechanistic studies have used low concentrations (1-300 ng/ml) of haptenated high-valency antigens (e.g., Dinitrophenyl $[DNP]_{26}$-BSA or trinitrophenyl $[TNP]_{26}$-BSA conjugates), which are type A antigens or high concentrations (0.5-5 μg/ml) of anti-IgE antibody (which has a valency of 2, similar to type A antigens) to activate IgE-sensitized mast cells. It is known that stronger activation signals are required for degranulation than for production of several cytokines such as IL-13, IL-6 and TNF [6]. It is noteworthy that many natural allergens consist of low-valency oligomers [7].

In addition to antigen-driven IgE molecules, there are natural IgEs produced in the absence of experimentally administered antigen. Natural IgE is spontaneously produced in T-cell-deficient and Germ-Free (GF) mice in an MHC class II cognate help-independent manner [8]. Production of natural IgE does not require secondary lymphoid structures or germinal center formation. Some natural IgEs have specificities directed against self-antigens such as phosphorylcholine. Natural IgE antibodies may play homeostatic roles in cancer surveillance and skin barrier defenses [9,10]. They may also regulate homeostasis of mast cells, as IgE molecules enhance mast cell survival and activity and surface levels of FcεRI [11-14]. A recent study showed that mice pretreated with glucocorticoids exhibit reduced IgE/antigen-induced anaphylaxis [15].

Histamine-Releasing Factor (HRF) has emerged as an Ig-binding alarmin. HRF, also known as Translationally Controlled Tumor Protein (TCTP) and fortilin, is an evolutionally conserved multifunctional protein. Intracellular HRF/TCTP is required for cell-cycle progression, proliferation, survival, malignant transformation and DNA repair [16,17]. On the other hand, HRF is found in bodily lavage fluids during the late phase of allergic reactions, implying its role in allergic diseases [18,19]. Human bronchial epithelial cells secrete HRF in response to allergens (e.g., House Dust Mite [HDM] allergens), cytokines (e.g., Th2, epithelial-derived and inflammatory cytokines), cell deaths and cell death-associated compounds (e.g., ATP and adenosine) and viral infection [20,21]. We previously showed that a subset of IgE and IgG molecules directly bind to HRF by low-affinity interactions between an Ig-Fab fragment and N-terminal 19 residues (N19) and a helical portion (H3) of HRF [22]. Recombinant proteins, particularly GST-N19 and HRF-2CA, which block HRF-IgE interactions prevent allergic phenotypes in IgE/mast cell-dependent animal models of asthma and food allergy [22-24].

These observations suggest that HRF is a humoral factor that promotes activation of mast cells and basophils by binding to FcεRI-bound IgE molecules. Consistent with this notion, HRF forms disulfide-linked multimers including a dimer and higher-order multimers, which may have the structural feature of repetitive epitopes in allergens, like type B or type C antigen mentioned

above [4,20,22,25,26]. Higher amounts of HRF are recovered from bronchoalveolar lavage fluids taken from patients with asthma or with idiopathic eosinophilic pneumonia, compared with healthy controls [19]. Furthermore, serum levels of HRF-reactive IgE are higher in human patients with asthma, food allergy, chronic spontaneous urticaria as well as animal models of these diseases, compared to healthy controls [22,23,27]. Interestingly, adult patients with severe asthma and pediatric asthmatic patients infected by rhinovirus have higher serum levels of HRF-reactive IgE than control individuals, suggesting that HRF may be involved in severe asthma and rhinovirus-induced asthma exacerbation [21]. HRF-reactive IgE and/or IgG molecules were also induced in mice by immunization with irrelevant antigens including ovalbumin or viral infection [21-23].

In this study, we investigated structural and immunological properties of Igs and HRF that determine their interactions and how these properties impact mast cell and basophil activity in both *in-vitro* and *In-vivo* allergic settings.

Methodology

EBV-Transformed Cord Blood B Cells

Mononuclear cells (MNCs; 1.8 x 10^6 cells) isolated by Ficoll-Hypaque density gradient from 6 ml of cord blood were infected with EBV-containing culture supernatant of the marmoset B95.8 B cell line for 1 hr at 37°C, washed and then plated into a 96-well plate at the cell density of ~1.8 x 10^4 cells/0.2 ml/well. As shown previously, this condition yielded transformed cells with variable growing rates in nearly every well [28,29]. After replacing 100 μl of each spent medium, which were saved, with 100 μl of fresh medium every week, the accumulated culture supernatants for a three-week period were subjected to ELISA for their reactivity with HRF and insulin (kindly provided by Dr. Hubert Tse) and immunofluorescence analysis for surface determinants on adult blood MNCs and GFP+ Jurkat cell line. This study was approved by the Institutional Review Board of University of Alabama at Birmingham.

Mice

All mice except GF mice were bred under specific pathogen-free condition in the animal facility of La Jolla Institute for Immunology (LJI) or RIKEN/IMS. Germ-free mice were bred by the Microbiome Core Facility of POSTECH. Animal experiments were approved by the Animal Use and Care Committees of LJI, RIKEN/IMS, POSTECH and CIEA and performed according to the NIH Guide for the Care and Use of Laboratory Animals. *FceRIa-/-* mice were donated by Takashi Saito (RIKEN/IMS). All genetically modified mice were backcrossed to a BALB/c or C57BL/6 background for more than 10 generations.

Mouse Anaphylactic Models

PSA: Mice were passively sensitized by i.p. injection of 200 μl at 10 μg/ml of anti-TNP IgE (C38-2 clone from BD Biosciences). 24 h later, PSA was induced by i.v injection of TNP_2-BSA or TNP_{26}-BSA (100 ◉l at 100 μg/ml). Some mice were pretreated i.v. with HRF inhibitor (100 μl at 1 mg/ml of HRF-2CA) 1 h before antigen stimulation. Body surface temperature was measured using infrared thermometer and and physical activity was monitered by video function of iPhone. Mcpt1 in serum was measured by ELISA at the end of experiment.

PCA: Mice were passively sensitized by intradermal injection of C38-2 IgE (10 μl at 1 mg/ml) or PBS at the ear. 24 h later, PCA was induced by i.v. injection of TNP_2-BSA or TNP_{26}-BSA (100 μl at 100 μg/ml) together with 1% Evans' blue dye. Some sensitized mice were pretreated i.v. with HRF inhibitor (100 μl at 1 mg/ml of HRF-2CA) 30 min before antigen injection. 30 min after antigen injection, mice were sacrificed. Ears were cut and weighed and then incubated in formamide overnight and spun down. Evans blue dye was measured by spectrophotometer (OD620 nm).

PSA with Humanized Mice

The PSA model using humanized mice were previously described [30]. In brief, 5x10^4 human CD34+ hematopoietic stem cells (StemExpress LLC., Folsom, CA, USA) were i.v. transplanted into X-ray-irradiated NOG hIL-3/hGM-CSF Tg mice to create the humanized mice [31]. To induce PSA, 1.6 μg of an anti-NP human/mouse chimeric IgE Ab (Serotec, Oxford, UK) was i.v. injected into the humanized mice at 15-17 weeks after HSC transplantation. 24 h after sensitization, 500 μg of NP_7-BSA or NP_{25}-BSA (Biosearch Technologies Inc., Novato, CA) was i.v. administered as a challenge. 30 min before the challenge, 200 or 300 μg of HRF-2CA was orally administered. Rectal body temperature was measured every 10 min after the antigen challenge.

Generation and Analyses of HRF-C172A Mice

To generate the targeting construct for HRF-C172A mice, a 2.0-kb 5′-arm containing exons 1-5 and a 2.1-kb 3′-arm containing exon 6 were PCR amplified from the mouse genomic DNA and cloned into pCR-Blunt vector (Thermofisher scientific) and sequenced. The primers for 5′-arm were: forward, aaaagatCTACCGGGACCTCATCAGCC; reverse, GTTCAAGGCTCTACTCTCCCAC. The primers for 3′-arm were: forward, aaatctaGATTGTGAGATCTTTATCCTGTGGG; reverse, aaagcggCCGCTAACCCCATAATCCCT. The site-directed mutagenesis of 3′ end of exon 5 to introduce alanine and stop codons were performed using primers: forward, gtgtGTAAGTATCTTTAAATTAGTAGTGTC; reverse, taagcTTTCTCCATCTCTAAGCC. The two arms were serially subcloned into the KpnI/BamHI and XbaI/NotI site of pPNT-loxp-neo targeting vector, respectively. The plasmid was linearized by Not I digestion and electroporated into 129xB6 F1-derived ES cells. Neomycin-resistant ES colonies were screened for the knock-in allele by PCR and Sanger sequencing. The selected ES cells were aggregated with diploid eight-cell stage embryos to produce chimera mice. The chimera mice were mated with CAG-Cre deleter strain to remove loxp-flanked neomycin cassette and further backcrossed to Balb/c background for 10 generations. The genotyping primers for C172A knockin strains were: forward, TAGAGATGGAGAAAGCTTAGT; reverse, GCATACATTATACGAAGTTATGG.

Histology and Hematology

Tissue samples were fixed in 7.5% formalin and embedded in paraffin. Blocks were cut into 5 μm thick sections, followed by staining with Hematoxylin and Eosin or Toluidine Blue. Whole sections were recorded using a Zeiss Axio Scan Z1 Slide Scanner. Mast cells were quantified using QuPath software version 0.2.0 using an average of five fields per tissue sample and 4 tissue samples per group [32].

Mice were briefly anesthetized with isoflurane before blood was collected via retro-orbital sampling with heparinized hematocrit capillary tubes. Approximately 100 μl of blood was collected from each mouse into EDTA-coated collection tubes. Complete blood count for each blood sample was obtained using an automatic hematology analyzer (Hemavet 950FS).
IgA from jejunum lumenal washes was quantified by ELISA.

Intestinal Permeability

Mice were orally gavaged with FITC-Dextran (4 kDa). 1 h later, blood was collected from mesenteric vein and the fluorescence of FITC-Dextran in sera was measure by SpectramaxM2.

Food Allergy Experiments

Food allergy experiments were performed according to our published study (23). Briefly, WT BALB/c and HRF-C172A mice were i.p. sensitized with OVA (50 μg/mouse) plus alum on days 0 and 14. On days 28, 30, 32 and 34, mice were intragastrically (i.g.) challenged with OVA (25 mg) or PBS (control). One day before the 1st challenge (day 27) and one day after the 3rd challenge (day 33), mice were starved for 3 h, then i.g. pretreated with HRF-2CA (100 μg/mouse). Body temperature and physical activity on each OVA challenge were monitored for 50 min after OVA challenge [33]. Feces were monitored for 1.5 h after OVA challenges. Diarrhea was scored (stool score) as follows: 0 = normal and dry pellet; 1, normal and wetter pellet; 2, wet and less-shaped pellet; 3, complete diarrhea. Student's t-test or AUC was used to compare temperature drops and diarrhea scores between groups. We previously tested the oral effect of HRF inhibitors (e.g., HRF-2CA and GST-N19) in this food allergy model with a hope to eventually develop an oral drug to prevent food allergy in humans. Dosages were determined by trial and error in our previous study [23].

Recombinant HRF Proteins

Mouse and human HRF-His_6 and HRF-2CA-His_6 expressed by pET-24a(+) plasmid were purified using ProBond resin (Invitrogen) and then using Superdex 200 Increase 10/300 column. PBS was used as the elution buffer at a flow rate of 0.5 ml/min. Purified HRF and HRF-2CA were dialyzed against PBS.

Enzyme-Linked Immunosorbent Assay (ELISA)

Mouse total IgE, IgG1 and IgG2b levels were analyzed using the following antibodies to capture the antibodies: purified rat anti-mouse IgE (BD Biosciences, Cat 553413); purified rat anti-mouse IgG1 (BD Biosciences, Cat 553440); rat anti-mouse IgG2b mAb (Abcam, Cat ab11566). 96-well ELISA plates were coated overnight with capturing antibodies (each at 1 μg/ml in 0.1 M carbonate

buffer [pH 9.5]). The plates were washed and blocked with 10% FCS. Next, diluted sera were incubated in the coated plates, after which bound immunoglobulins were detected by incubation with biotinylated detection antibodies followed with HRP-conjugated streptavidin (BD Biosciences). Color was developed using TMB substrate (Biolegend) and absorbance at 450 nm was measured and corrected with absorbance at 570 nm.

HRF was measured using anti-TPT1/TCTP antibody (Novus Biologicals, Cat# H00007178- M06, clone 2A3) for capturing and anti-TPT1/TCTP antibody (self-biotinylated mAb, Novus Biologicals, Cat# H00007178-M03, clone 2C4) and streptavidin-β-Gal conjugate (Roche, Cat# 11112481001) for detection. After incubation with streptavidin-β-Gal conjugate and washing, ELISA wells were incubated with 0.2 mM 4-Methylumbelliferyl-β-D-galactopyranoside (4-MU-Gal, Sigma- Aldrich, Cat# M1633) for 1 h at 37°C. Fluorescence was measured at excitation of 365 nm and emission of 445 nm.

HRF-reactive IgE was measured using in-house ELISAs: ELISA wells were coated with 10 μg/ml recombinant human or mouse HRF-His_6 in 0.1 M sodium carbonate buffer (pH 9.5) for overnight at Room Temperature (RT). After washings, the wells were blocked with ImmunoBlock (DS Pharma Biomedical, Japan, Cat# CTKN001) for 2 h. The wells were washed and incubated with IgE samples or control for 2 h. After washings, the plates were incubated with 1 μg/ml biotin anti-human IgE (anti-mouse IgE) for 1 h at RT. Then the wells were washed and incubated with streptavidin-β-Gal conjugate, followed washings and incubation with 0.2 mM 4-MU-Gal for 1 or 2 h. Fluorescence was measured at excitation of 365 nm and emission of 450 nm. HRF-reactive IgG was similarly analyzed except for the use of biotin anti-human IgGs or biotin anti-mouse IgGs instead of anti-human IgE.

Mast Cell Culture and Stimulation

Femurs of mice were aseptically removed and bone marrow cells were cultured in RPMI1640 medium supplemented with mouse IL-3, 10% FCS, 100 μg/ml penicillin and 100 U/ml streptomycin at 37°C in a humidified incubator with 5% CO2. Cells cultured with weekly media changes became >90% positive for c-Kit^+ and $Fc\varepsilon RI^+$ (by flow cytometry) after 5-7 weeks. These cells (termed bone marrow-derived mast cells [BMMCs]) were used for overnight sensitization with mouse IgE (0.5 μg/ml), being washed and then stimulated with antigen. Alternatively, unsensitized or IgE-sensitized BMMCs were stimulated with Substance P (100 μM), compound 48/80 (50 μg/ml), PMA (50 ng/ml) + Ionomycin (0.5 μM) or LPS (1 μM) for 30 min. Degranulation was quantified after 30 min stimulation (unless otherwise mentioned) by cell surface expression of CD63 by flow cytometry or by β-hexosaminidase activity of culture supernatant. Cytokine production was measured after 16 h stimulation.

siRNA-Mediated Knockdown

RAW264.7 cells in 96-well plates were transfected with siRNAs (4 different siRNAs per target gene, from LJI siRNA Center) with the help of Lipofectamine (Thermo Fisher). Two days later, the cells were analyzed for expression of target mRNAs by qRT-PCR and proteins by western blotting. Reduced expression of target mRNAs by at least 70% was confirmed by qRT-PCR.

Western Blot Analysis

Culture supernatants and cell lysates were analyzed by western blotting. Proteins in these samples were separated by SDS-PAGE (under reducing and non-reducing conditions) and then transferred to polyvinylidene difluoride membranes. Antibodies to the following proteins were used as primary antibody to detect them: HRF (anti-TPT1 mAb clone 2C4, Catalog #, H00007178-M03) from Abnova was used unless otherwise depicted), Flotillin-1, CD9, Annexin and CD54 (Cell Signaling Technology). Horseradish peroxidase-linked anti-mouse IgG Ab and Horseradish peroxidase-linked anti-rabbit IgG Ab were used as secondary antibody.

Quantitative Analysis of mRNA

Total RNA was prepared using TRIzol (ThermoFisher Scientific) according to the manufacturer's instruction and first-strand cDNA synthesis was carried out using SuperScript II Reverse Transcriptase (Invitrogen). mRNA expression was quantified by real-time PCR (BioRad) using SYBR Green I master reagent (Roche Diagnostics). The sequences of the synthetic oligonucleotides used as primers are as follows: for detection of TCTP forward, 5′- GATGAGATGTTCTCCGACA -3′, reverse, 5′- TGTTACCTTCTGTCCTACTG -3′; for detection of mouse18S rRNA forward, 5′- CTACCACATCCAAGGAAGCA -3′, reverse, 5′- TTTTTCGTCACTACCTCCCCG -3

Prediction of Protein Structures

The ColabFold v1.5.2 interface of AlphaFold2 and AlphaFold2-multimer v3 (34) was used to predict 3D structures of protein monomers and complexes (https://colab.research.google.com/github/sokrypton/ColabFold/blob/main/AlphaFold2.ipynb) with the following settings: num_relax=5, template_mode=none, msa_mode = mmseqs2_uniref_env, pair_mode=unpaired_paired, model_type=auto, num_recycles=auto, recycle_early_stop_tolerance=auto, pairing strategy=complete for complexes involving only mouse proteins or greedy for complexes involving proteins of two or more species, max_msa=auto, num_seeds=1, use_dropout=false. The results were visualized with PyMOL (version 2.5.2). The solvation free energy gain (ΔiG), BSA and amino acid residues in the protein interfaces were calculated using PISA (35) (https://www.ebi.ac.uk/msd-srv/prot_int/pistart.html).

Statistical Analysis

Statistical analysis was performed using Prism 9.4.1 for Mac software (GraphPad). Data are presented as mean ± SEM in all figure parts in which error bars are shown. Groups were analyzed by 2-tailed Student's t test, paired t test and 2-way ANOVA, unless otherwise indicated. $P < 0.05$ was considered statistically significant.

Results

HRF Binds to Both Natural and Antigen-Driven Antibodies

To date, studies on HRF reactivity have been limited to antigen-driven specific IgE and IgG antibodies [22]. It is interesting to investigate whether HRF recognizes natural antibodies, some of which may have germline or quasi-germline V(D)J sequences. First, we tested whether HRF interacts with natural IgE in GF mice. As shown previously serum levels of total IgE and total IgG1, but not total IgG2b, were higher in GF than in Specific Pathogen-Free (SPF) mice (Fig. 1) [28,29]. Levels of HRF-reactive IgE and HRF-reactive IgG1, but not HRF-reactive IgG2b, were also higher in GF than in SPF mice (Fig. 1). However, serum levels of HRF were similar between GF and SPF mice (Fig. 1). Second, as the large majority of natural antibodies belongs to the IgM isotype, we tested whether HRF interacts with IgM molecules produced by Epstein-Barr Virus (EBV)-transformed human cord blood B cells [30,31]. Similar to antigen-driven IgE and IgG antibodies, a subset of these IgM molecules (14.6% to 80%, depending on without or with adding +/- samples) also bound HRF (Fig. 1,Table S1). Some of these HRF-reactive IgM molecules also recognized insulin and cell surface molecules (Table S1), indicative of the polyreactivity characteristic of natural antibodies [30,32]. Third, we tested whether allergen-specific human IgE molecules bind to HRF. A substantial subset (at least 20 or 50%) of human monoclonal IgEs specific to HDM or peanut component allergens also bound HRF (Fig. S1) [33]. Finally, we tested whether immunization in general induces HRF-specific antibody responses, as various conditions induce HRF secretion [19,20,22,23]. HRF-reactive IgG1 molecules were isolated by M13 phage display libraries generated from mice immunized with irrelevant antigens such as L-SIGN/Fc, DC-SIGN/Fc, CD80/Fc-His, CD86/Fc-His and bacterial LPS. A large panel of antibodies isolated from four rounds of panning of four different libraries on immobilized mouse HRF (mHRF) represented 13 clusters of 37 antibodies classified by heavy-chain CDR3 sequences (Table S2). Inspection of these antibodies indicates that there is a wide range (0-20 mutations) of nonsynonymous mutations in the VH region of these antibodies, including a small number of germline and quasi-germline IgG1 antibodies with HRF-reactivity (e.g., A-C9, C-G3, A-H2), as well as antibodies with as many as 15 or 16 nonsynonymous mutations (e.g., cluster 2); that there is also a wide range (>100 fold) of HRF binding activity among these antibodies, some of which exhibit high HRF reactivity and somatic hypermutation (SHM) (e.g., D-G10 and D-F9) (Table S2); and that HRF-reactive IgG1 antibodies have more nonsynonymous than synonymous mutations except for two clones and that some V_H genes are tightly associated with specific J gene segments (e.g., WECQ with J3 in 10 out of 10 HRF-reactive IgG1 clones shown in Table S3). Therefore, the results collectively suggest that, in addition to antigen-driven IgE and IgGs, HRF recognizes various natural IgE, IgG1 and IgM antibodies, some of which show polyreactivity to other proteins and numerous irrelevant antigen-driven IgG1 antibodies with a wide range of HRF affinity and SHM, which aligns with those from germline/quasi-germline VH sequences to seemingly highly mutated HRF-specific V_H sequences [22].

HRF spontaneously multimerizes extracellularly, but requires oxidoreductases for its dimerization intracellularly

Since the presence of HRF dimers and higher-order multimers were previously shown, we next explored how HRF is multimerized [20,25]. Mouse and human HRF molecules are highly conserved proteins of 172 amino acids with two cysteine residues, C28 and C172. Recombinant Wild-Type (WT) as well as C28A, C172A and 2CA (C28A/C172A double mutant) mHRF molecules were expressed in *E. coli*. Purified (~98%) WT mHRF monomers in Phosphate Buffered Saline (PBS) after storage at 37°C for 90 min formed a ladder of several bands on SDS-PAGE under non-reducing conditions (Fig. 2A, Left). Longer incubation

(3 days at 37°C in Fig. 2A, Right) or 3 h at 70°C (data not shown) facilitated HRF multimerization even more extensively. C28A mutant behaved similarly but multimerized more slowly (Fig. 2). By contrast, C172A and 2CA mutants did not form multimers, consistent with the 3-Dimentional (3D) structure of a human HRF (hHRF) dimer disulfide-linked via C172 residues from two monomers [25]. Reflecting the high-molecular-weight nature, WT, but not 2CA, HRF solutions looked slightly turbid (Fig. 2). Conversion of WT mHRF monomers to multimers was not affected by the presence of HRF inhibitor (i.e., HRF-2CA) or co-incubation of mHRF with anti-N19 mAb (renamed F7-1 to avoid mix-ups with SPE-7 IgE) (24) or isotype control mAb at 37°C (data not shown). These results show that multimerization of mHRF through disulfide linkages involving C172 and C28 residues does not require any enzyme in an aqueous solution. By contrast, dimerization of mHRF within the cell required endoplasmic reticulum-resident oxidoreductases Erol1 and Erol1b in a murine macrophage line under unstimulated or allergy-promoting conditions, as it was inhibited by short-interfering RNAs (siRNAs) targeting these proteins (Fig. 2). This is plausible with the highly reducing environment of the cytosol compared with the oxidative extracellular environment [34,35]. We also expressed hHRF-His_6 in HEK293T human embryonic kidney cells. Similar to *E.coli*-produced mHRF, purified hHRF-His_6 produced in HEK293T cells also formed multimers non-enzymatically (Fig. 2). We engineered genetically modified mice with HRF-C172A mutation to abrogate multimerization of HRF (Fig. S2). Homozygous HRF-C172A mice backcrossed with BALB/c or C57BL/6 mice for 10 generations appeared normal. Their organs (Fig. S2), blood cells (Fig. S2) and immune phenotypes of splenic (Fig. S2) and mesenteric lymph nodes (Fig. S2F) seemed to be largely normal. Bone marrow cells from HRF-C172A mice proliferated and differentiated into mast cells (BMMCs) in IL-3/stem cell factor-containing medium as well as those from WT mice (Fig. S3). These BMMCs exhibited growth factor depletion-induced apoptosis similar to WT BMMCs (Fig. S3). IgE/antigen-stimulated BMMCs derived from HRF-C172A mice degranulated (Fig. S3) and produced cytokines (IL-13 and TNF) somewhat better than WT controls (Fig. S3). The results collectively imply that the intracellular functions of HRF/TCTP are executed by the predominant form of HRF monomer, while the extracellular functions are performed by HRF multimers.

HRF multimers enhance antigen/IgE-mediated activation of mast cells at suboptimal antigen doses

In light of the non-enzymatic multimerization of HRF outside the cell, we addressed whether HRF dimers and multimers affect antigen-induced activation of mast cells. Initially, HRF dimers were used as they seemed to be a unit of multimerization and purification of individual multimers with higher molecular weights was extremely difficult. We also used mixtures of HRF multimers (similar to those shown in Fig. 2) and their effects on mast cell activation induced by low-valency haptenated antigens (e.g., TNP_3-BSA or DNP_3-BSA) and supernatural high-valency antigens (e.g., TNP_{26}-BSA or DNP_{26}-BSA). Incubation of HRF dimers or multimers alone in HRF-reactive IgE (i.e., anti-TNP IgE C38-2)-sensitized WT BMMCs or unsensitized WT BMMCs for 30 min did not induce degranulation (Fig. 3 and S4). Up to 25 or 50 μg/ml of HRF dimers did not affect antigen-induced degranulation in at least 5 independent experiments, but they consistently enhanced cytokine (IL-13) production in an antigen dose-dependent manner in HRF-reactive IgE-sensitized BMMCs (Fig. 3B), in line with stronger FcεRI stimulation being required for degranulation than for cytokine production [6,36]. In these experiments, degranulation was assayed 30 min after simultaneous stimulation with antigen and HRF dimers while cytokine production was measured after 16-24 h stimulation. Longer (>30 min) incubation converted HRF dimers to multimers (Fig. S4). We next stimulated C38-2 IgE-sensitized BMMCs with antigen in the presence of HRF multimers. Under this condition, antigen-induced degranulation and cytokine production were enhanced by HRF multimers at suboptimal antigen concentrations, whose relative effects were similar at their highest enhancing effects of more than 3 folds, when stimulated with low-valency (1 ng/ml TNP_3-BSA) or high-valency (0.1 ng/ml TNP_{26}-BSA) antigen (Fig. 3,S4). As expected, activating effects of HRF multimers were not seen in Fcer1a-/- BMMCs deficient in FcεRIα (data not shown). These results suggest that HRF multimers lower the threshold of antigen concentrations required to fully activate mast cells and enhance the magnitude of activation and that HRF dimers can enhance antigen/IgE-induced cytokine production, but not degranulation. By contrast, when WT BMMCs were sensitized with an HRF-nonreactive IgE (e.g., anti-DNP IgE DNP-ε-206 or SPE-7), antigen (DNP_2-BSA or DNP_{26}-BSA)-induced activation of BMMCs was not enhanced by HRF dimers or multimers (Fig. S5). In other control experiments, activation of WT and FcεRIα-deficient mast cells via Mrgprb2, a G-protein-coupled receptor for several positively charged chemicals and substance P, was not enhanced by HRF multimers and the strong activator of Mrgprb2, compound 48/80, induced full degranulation in both mast cells, which was not further affected by HRF multimers (Fig. S5) [37]. Activation of mast cells by Phorbol 12-Myristate 13-Acetate (PMA) and ionomycin, which circumvents the FcεRI-proximal events, was little affected by HRF multimers or FcεRIα deficiency, while LPS failed to induce degranulation with or without HRF multimers (Fig. S5). These *in-vitro* studies suggest that interactions between HRF multimers and FcεRI-bound IgE molecules render mast cells more sensitive and more responsive to suboptimal antigen concentrations.

Predicted structures for interactions between HRF and HRF-reactive antibodies

Amino acid sequences of numerous mHRF-reactive IgG1 molecules are now known (Tables S2 and S3), while only a few hHRF-reactive IgG or IgE sequences are known [22]. We and others reported 3D structures of human and mouse HRF monomers [25,38]. While we reported a crystal structure of a hHRF homodimer (hHRF-2 dimer) with a C172-C172 disulfide linkage, the structure of a disulfide-linked mHRF dimer is not known [25]. Advancement in the prediction of molecular structures was made by artificial intelligence-based programs, particularly AlphaFold2 [39,40]. Using a web-application of AlphaFold2, the ColabFold, first, 3D structures of mHRF and hHRF monomers and dimers were predicted [41]. Predicted structures of HRF monomers (Fig. S6) and dimers (Fig. S6) were quite similar to the crystal structures revealed by X-ray crystallography, particularly in the core structures except for the disordered loop portions [25]. Next, complexes containing an mHRF monomer and the VH and VL domains (VH/VL)1 were predicted (Fig. S6 and Table S4). The AlphaFold2 predicts protein structures in two steps: "unrelaxed" models are predicted by AlphaFold2 core first and then Assisted Model Building with Energy Refinement (AMBER) relaxation is performed to refine the atomic positions if desired. We noticed that there were no major changes in amino acid residues that have Buried Surface Area (BSA) upon complex formation before and after AMBER relaxation. However, the predicted polar contacts including hydrogen bonds and salt bridges were altered. Therefore, we focused on the buried surface to find the interacting amino acids. The solvation free energy gains (ΔiG) for VH-VL interfaces were similar across the predicted complexes except for the aberrantly folded predictions, implying the stable coordination of VH/VL domains (Table S4). The (VH/VL)1 domains of the high-affinity mouse IgG1 clones B-G7 and D-G10 (Table S2) were predicted to have interactions with the different residues of the N19 region of mHRF (Fig. S6D and Table S4). By contrast, HRF-nonreactive VH/VL molecules from HRF-nonreactive SPE-7 IgE were predicted to interact with the other sites of mHRF, without a substantial ΔiG for the VL-contacting interface (Fig. S6D and Table S4) [22]. Since AlphaFold2 gives candidates even when the molecules do not make a complex, the results imply that this predicted interaction is not a specific one. Furthermore, AlphaFold2 predicted specific interactions between the N19 portion of GST-N19 (the antigen used for immunization) and the Fab portion of anti-N19 mAb F7-1 (24), but not those between the N19 portion and SPE-7 IgE (Fig. S6, Table S4). We further attempted to obtain predicted complexes containing a mHRF dimer and (VH/VL)2 domains of B-G7 and D-G10 clones. Because mHRF dimer conformation was not stable in the predicted structures in these 6-mer complex (data not shown), we used an imaginary single-chain mHRF dimer (termed scdmHRF), consisting of two mHRF monomers made by connecting two peptide chains with a linker peptide Gly-Ser-Gly-Ser-Gly (Fig. S6). Although the predicted structure of this scdmHRF was similar to that of the disulfide-linked mHRF dimer, the scdmHRF's interfaces with (VH/VL)2 domains of B-G7 and D-G10 were not the same as those of mHRF monomer, implying the limitation of the AlphaFold2. However, the interface contained amino acids of N19 region in some of the predicted complexes (Fig. S6G). Furthermore, scdmHRF in one of the predicted complexes with the D-G10 (VH/VL)2 contained C172-C349 (corresponding to C172 of the latter mHRF part) disulfide linkage (Fig. S6H). In this complex, the two mHRF component was twisted when bound by D-G10 (VH/VL)2. Considering the fact that the interaction of dimeric interfaces of HRF are not strong, it raises the possibility that the mHRF dimer exposes two binding sites when the two component are twisted around the disulfide-linked C172 [42]. The above 3D prediction analyses, in addition to numerous mutations in the coding sequences, which should have been introduced by SHM, suggest that high-affinity antibodies B-G7 and D-G10 could be HRF-specific antibodies with VH/VL interactions involving the N19 region of HRF. Parenthetically, differences in VH/VL interacting sites within the N19 region between B-G7 and D-G10 indicate the presence of multiple epitopes in this short region of HRF.

HRF plays an essential role for anaphylaxis and food allergy in mice

Next, we addressed whether *in-vivo* allergic reactions reflect *in-vitro* HRF effects on FcεRI-mediated activation of mast cells, using murine models of Passive Systemic Anaphylaxis (PSA), Passive Cutaneous Anaphylaxis (PCA) and food allergy. Both PSA and PCA are dependent on antigen, antigen-specific IgE and FcεRI [43,44]. PSA was recently shown to be dependent on connective tissue-type mast cells [45]. While more complex in its pathogenic mechanisms, food allergy also depends on IgE, FcεRI and mast cells [46-48]. In PSA, mice passively sensitized with HRF-reactive anti-TNP IgE (C38-2) were challenged with antigen 24 h later. HRF inhibitor (i.e., HRF-2CA) dramatically reversed TNP_2-BSA-induced hypothermia and low physical activity in WT mice (Fig. 4). These anaphylactic signs were also drastically reduced in HRF-C172A mice compared with WT mice (Fig. 4). Consistent with the critical role of mast cells in PSA, serum levels of Mcpt1, a mast cell protease, were reduced by HRF inhibitor or HRF-C172A mutation (Fig. 4). The effect of HRF inhibitor or HRF-C172A mutation on PSA was smaller when high-valency antigen TNP_{26}-BSA was used (Fig. 4C, D). There seemed to be stronger effects of HRF-C172A mutation than those of HRF-2CA on temperature drop. However, these differences may not be of inherent nature between effects of HRF-2CA administration and HRF-C172A mutation, as the differences could be applied to a fixed amount of HRF-2CA administered. When HRF-nonreactive anti-DNP

IgE (SPE-7 or DNP-ε-206) was used for sensitization, no effects of HRF inhibitor or HRF-C172A mutation were observed irrespective of antigen valency TNP_2-BSA or TNP_{26}-BSA (Fig. S5C, D), as expected. Consistent with the *in-vitro* data, hypothermia and low physical activity as well as increased Mcpt1 induced by intravenous injection of compound 48/80 were not reduced by HRF inhibitor (Fig. 4E). Next, when TNP_2-BSA was used in PCA challenge on mice passively sensitized with HRF-reactive IgE, PCA reaction in WT mice was substantially reduced by HRF-2CA, as measured by extravasation of Evans' Blue dye (Fig. 5). Reduced PCA reaction was also observed in HRF-C172A mice compared with WT mice (Fig. 5). By contrast, effects of high-valency antigen (TNP_{26}-BSA) challenge in PCA were not affected by HRF-2CA in WT mice (Fig. 5) or by HRF-C172A mutation (Fig. 5D). When sensitized with the HRF-nonreactive IgE DNP-ε-206, PCA induced with DNP_{26}-BSA was not affected by HRF inhibitor in WT or HRF-C172A mutation (Fig. S5). Compound 48/80-induced vascular permeability at dermal injection sites was similar between WT and HRF-C172A mice (Fig. 5E). These PSA and PCA results demonstrate the essential function of HRF to enhance the antigen (particularly low-valency antigen)/IgE-mediated activation of mast cells. Our previous studies showed that HRF inhibitors reduced the phenotypes of Ovalbumin (OVA)-induced, IgE/mast cell-dependent food allergy, e.g., diarrhea, hypothermia and reduced physical activity [23,24]. While we confirmed these results by administering HRF-2CA to WT mice (Fig. 6), we also evaluated the role of HRF multimerization using HRF-C172A mice (Fig. 6). Mast cell numbers in the small intestine, intestinal permeability in the small intestine and IgA levels in jejunum were indistinguishable at baseline between WT and HRF-C172A mice (Fig. S7). However, the mutant mice were protected from allergen-induced hypothermia, low physical activity and diarrhea unlike WT mice (Fig. 6). These results also support the critical role of HRF in OVA-induced food allergy.

HRF plays a significant role for anaphylaxis in humanized mice

HRF multimers are present not only in mice, but also in human nasal washes, saliva and tears [20]. Thus, we tested whether hHRF has a similar effect on mast cell activation. Preliminary PSA experiments were performed with humanized NOG hIL3/hGM mice (Fig. 7), which expressed human mast cells and basophils in addition to endogenous murine mast cells and basophils [49]. These mice were sensitized with a 4-hydroxy-3-nitrophenylacetyl (NP)-specific human IgE and challenged with NP_7-BSA next day. Only humanized, but not non-humanized, mice responded to antigen challenges by hypothermia (data not shown), in line with the prior observation that human IgE does not interact with rodent FcεRI [50]. In an experiment using a batch of humanized mice, control mice died at early time points (3 mice within 20 min and one mouse within 30 min) after NP_7-BSA challenge. By contrast, when mice were orally pretreated with 200 μg of HRF-2CA before antigen challenge, only one mouse died at a later time point (more than 40 min) and the other three mice survived for the experimental course of 60 min (Fig. 7B). In the next experiment using another batch of humanized mice, oral pretreatment with 300 μg of HRF-2CA protected all 6 mice very well from NP_7-BSA-induced hypothermia (Fig. 7C). However, when NP_{25}-BSA, a supernatural high-valency antigen, was used in place of NP_7-BSA, effects of HRF-2CA treatment were not seen (Fig. 7D). Thus, we conclude that hypothermia and anaphylactic deaths induced by an antigen of an intermediate valency are reduced by treatment of HRF-2CA before antigen challenge. These results suggest a critical role of HRF in IgE-mediated human anaphylaxis.

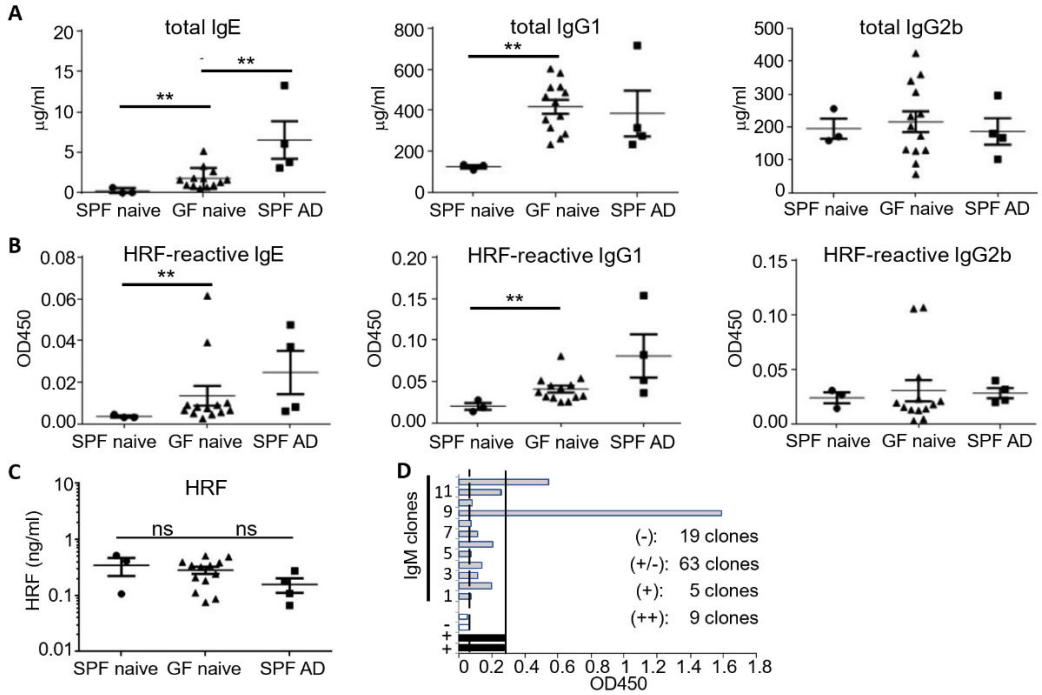

Figure 1: HRF can bind to natural antibodies of IgM, IgG1 and IgE classes. Total IgE, IgG1 and IgG2b (A) as well as HRF-reactive IgE, IgG1 and IgG2b (B) were quantified in sera from naïve GF (n=13) and SPF (n=3) mice. (C) HRF in serum was also quantified in these mice. SPF mice (n=4) with induced atopic dermatitis-like skin inflammation served as a control with high IgE and IgG1. (D) IgM molecules derived from 96 different EBV-transformed cord blood B cell cultures were tested for their reactivities with HRF by ELISA. HRF reactivity of randomly chosen 12 clones are shown along with HRF-reactive and HRF-nonreactive control IgEs. The broken line indicates negative HRF-reactivity and the unbroken line indicates positive HRF reactivity. Numbers of nonreactive (-), ambiguous (±, OD_{450} values between HRF-nonreactive and HRF-reactive IgEs), single positive (+, OD_{450} values between HRF-reactive and 0.8) and double positive (++, OD_{450} values > 0.8) clones are also indicated.

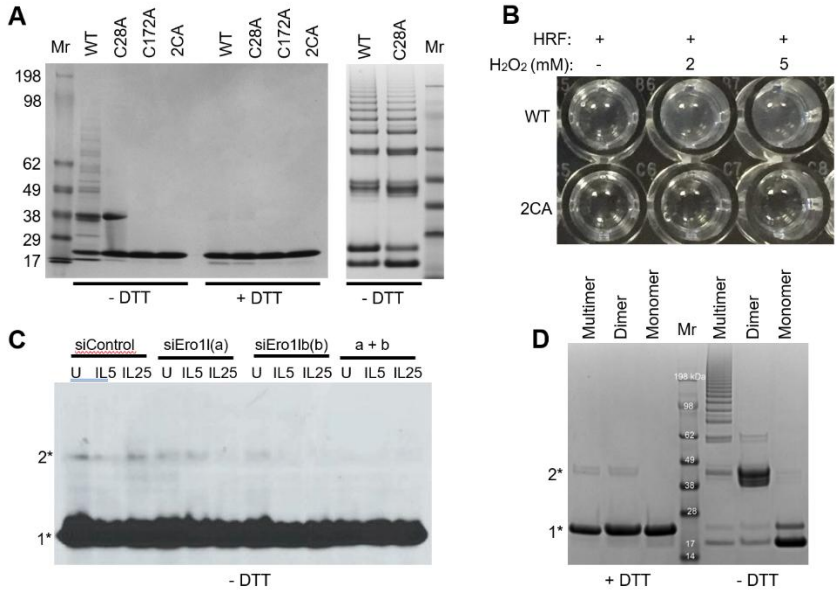

Figure 2: Non-enzymatic conversion of HRF monomers to disulfide-linked multimers takes place via Cys172 extracellularly. (A) Recombinant mouse WT, C28A, C172A and 2CA HRF molecules were expressed in *E. coli* and purified. Purified monomers were incubated at 37°C for 1.5 h (Left) or 3 days (Right). After incubation, samples were diluted to 0.5 µg/ml with PBS and boiled with either −DTT or +DTT sample buffer and analyzed by SDS-PAGE and followed by Coomassie Brilliant Blue staining. (B) Purified mouse WT, but not 2CA, HRF solutions in phosphate-buffered saline (PBS) with or without oxidizing condition by H_2O_2 had a turbid appearance. (C) RAW264.7 cells were transfected with siRNAs targeting Ero1l, Ero1lb or both (siControl,

non-targeting siRNAs) and stimulated by the indicated cytokine. U, unstimulated. Cell lysates were analyzed by nonreducing SDS-PAGE, followed by western blotting with anti-HRF antibody. Given similar knockdown efficiency for Ero1l and Ero1lb (>60%), Ero1lb seems to play a more important role in HRF dimerization than Ero1l. 1, monomer; 2, dimer. (D) hHRF monomers expressed in HEK293T cells were also converted to multimers in PBS.

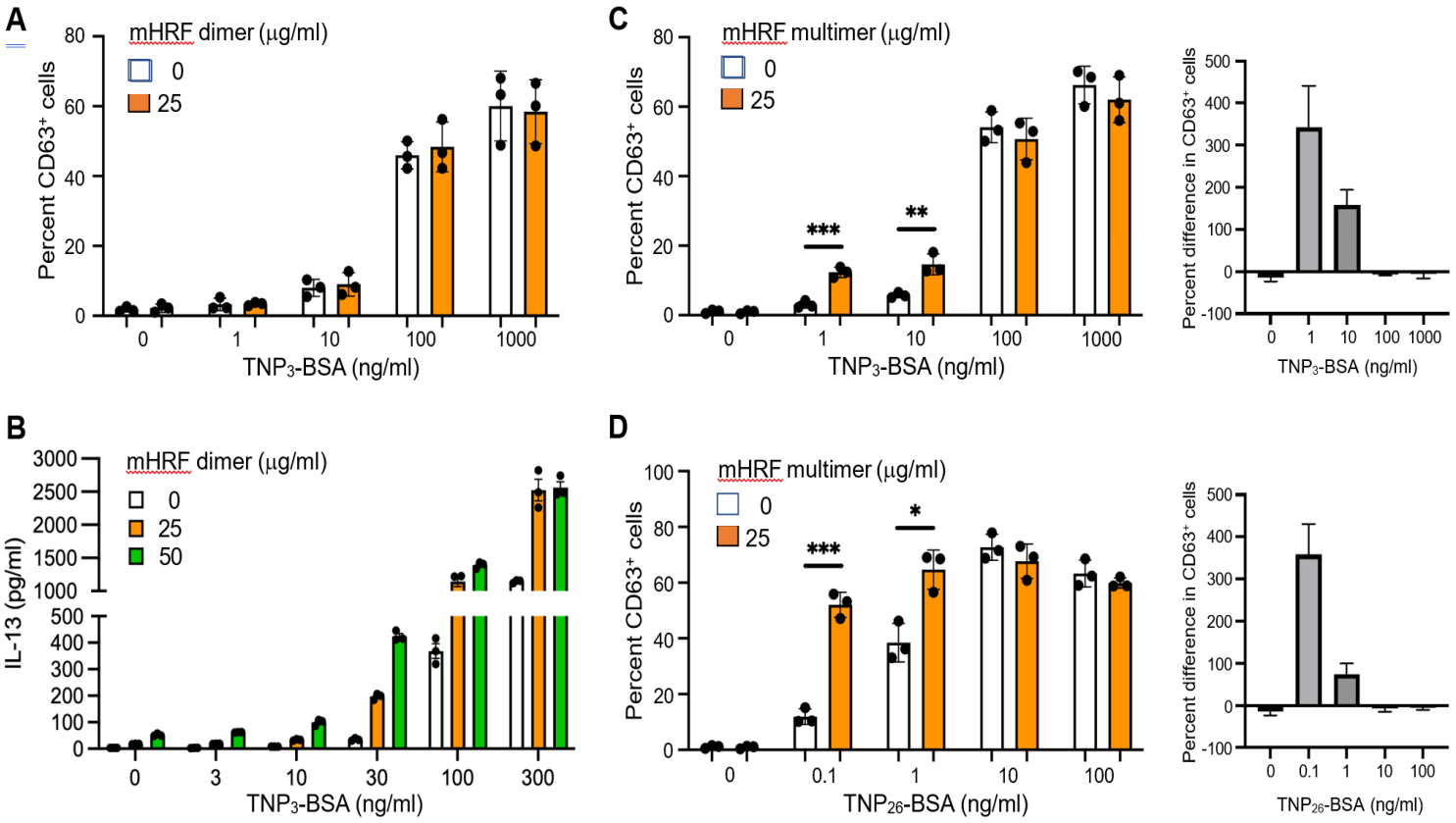

Figure 3: HRF multimers enhance antigen sensitivity and amplitude of activation levels of mast cells at suboptimal antigen concentrations. (A-D) BMMCs were sensitized overnight with HRF-reactive anti-TNP IgE C38-2 (0.5 μg/ml), then incubated with the indicated concentrations of mHRF dimer (A,B) or multimers (C,D) in the presence of the indicated concentrations of TNP_3-BSA or TNP_{26}-BSA for 30 min for the measurement of degranulation (A,C,D) or for 16 h for the measurement of IL-13 secretion (B). Experiments were done in triplicate. (A,C,D) Surface expression of CD63 was measured by flow cytometry as a surrogate of degranulation. Percent difference in $CD63^+$ cells due to the absence vs. presence of mHRF multimers are shown on the Right. (B) IL-13 in culture supernatants was quantified by ELISA. EC_{50} of antigen for IL-13 secretion: 156 ng/ml for 0 μg/ml mHRF dimer; 124 ng/ml for 25 μg/ml mHRF dimer; 92 ng/ml for 50 μg/ml mHRF dimer. *, $p<0.05$, **, $p<0.01$, ***, $p<0.001$ by Student's t test.

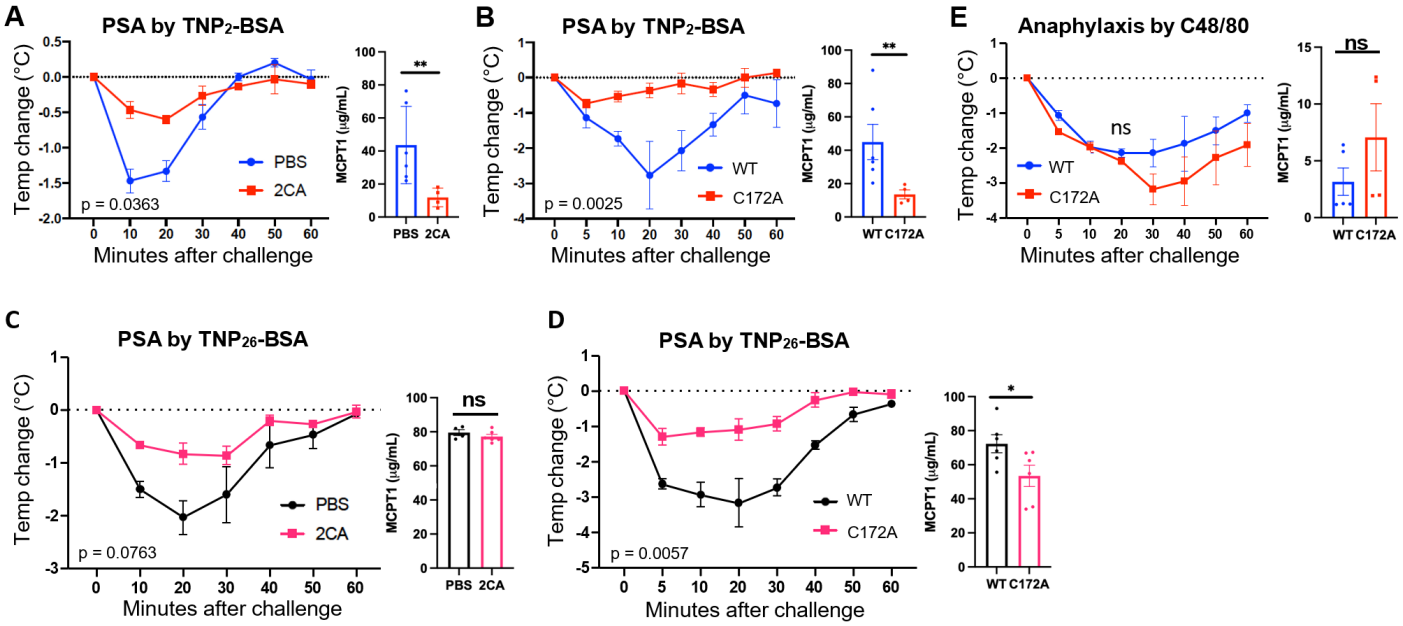

Figure 4: Reduced PSA reactions by HRF inhibitor and HRF-C172A mutation. (A,B) Mice were passively sensitized with anti-TNP IgE C38-2. 24 h later, PSA was induced by low-valency antigen TNP_2-BSA with (n=4) or without (n=6) HRF inhibitor pretreatment in WT mice (A) or HRF-C172A mice (B). Body surface temperature was measured using infrared thermometer (A,B) and Mcpt1 in serum was measured by ELISA (Right panels). (C,D) Effects of HRF inhibitor (C, n=4 each for PBS and HRF-2CA) or HRF-C172A mutation (D, n=4 for WT; n=6 for HRF-C172A) on PSA-induced hypothermia was measured when high-valency antigen TNP_{26}-BSA was used. (E) Anaphylaxis was induced with compound 48/80 (WT, n=5; HRF-C172A, n=4). Temperature changes were monitored and serum Mcpt1 was quantified. P values for temperature changes analyzed by 2-way ANOVA.

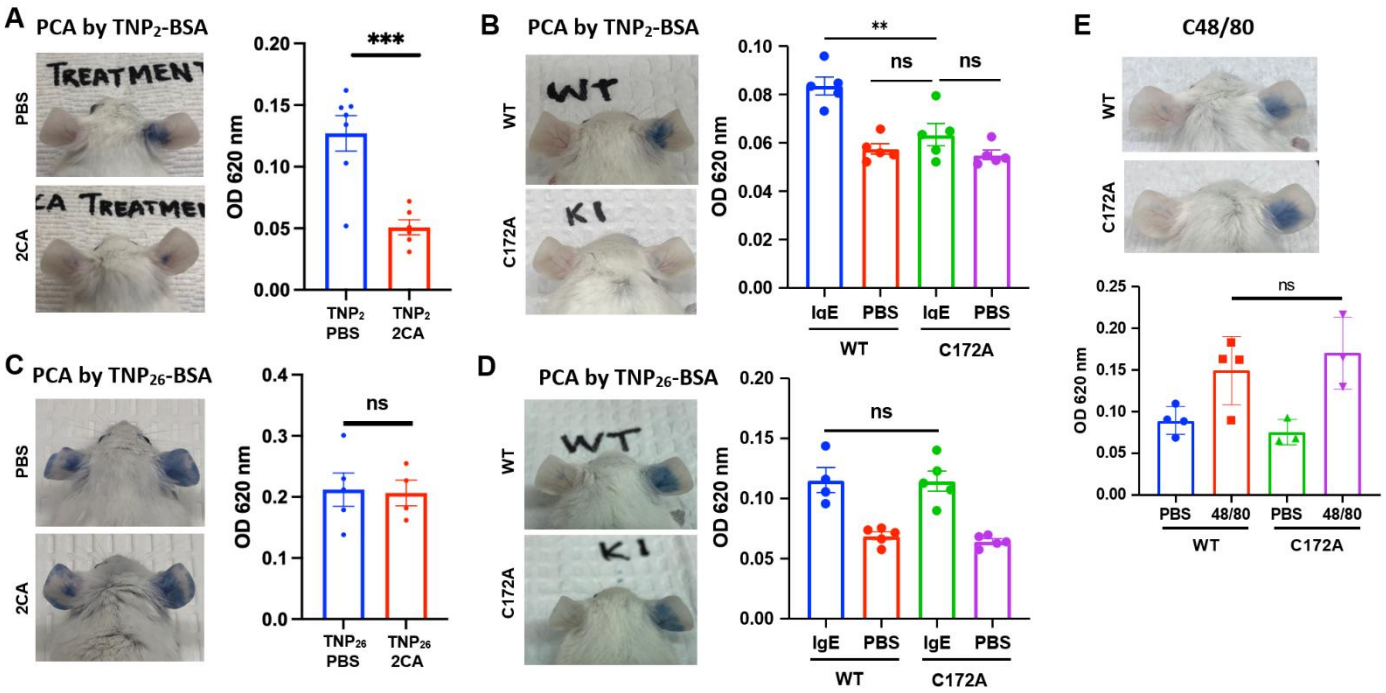

Figure 5: Reduced PCA reactions by HRF inhibitor and HRF-C172A mutation. (A,B) 24 h after passive sensitization by intradermal injection of C38-2 IgE or PBS at the ear, PCA was induced by low-valency antigen TNP_2-BSA (or PBS as a negative control) together with Evans' blue dye with or without HRF inhibitor pretreatment in WT mice (A, PBS, n=7; HRF-2CA, n=6) or HRF-C172A mice (B, WT: IgE, n=5; PBS, n=6; HRF-C172A: IgE, n=5; PBS, n=5). Dye extravasation was quantified. (C,D) Dye

extravasation induced by high-valency antigen TNP_{26}-BSA challenge in PCA was measured in HRF inhibitor-treated (n=4) vs. untreated (n=5) WT mice and in WT (IgE, n=4; PBS, n=5) vs. HRF-C172A (IgE, n=5; PBS, n=5) mice. (E) Dye extravasation induced by compound 48/80 was compared between WT (PBS, n=4; C48/80, n=4) and HRF-C172A (PBS, n=3; C48/80, n=3) mice.

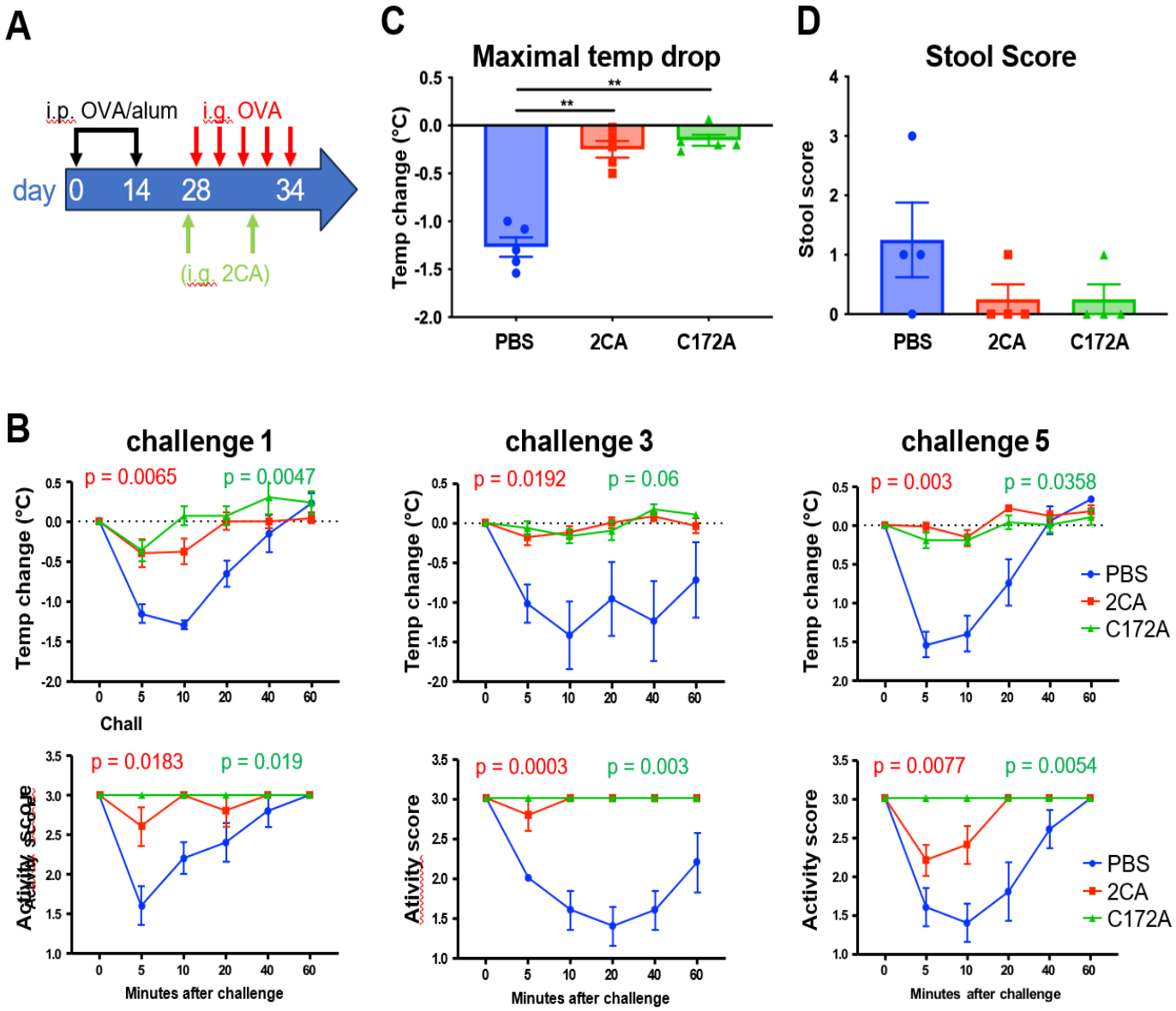

Figure 6: HRF-C172A mice are protected from OVA-induced food allergy. WT (n=11) and HRF-C172A (n=5) mice were subjected to the OVA sensitization and OVA challenge model of food allergy. Some OVA-sensitized WT mice were pretreated with HRF-2CA (2CA, n=6; PBS, n=5) one day after the first and third OVA challenges. (A) Experimental scheme. Body temperature (B,C), physical activity (B) and stool score (D) of the mice were monitored. P values by 2-way ANOVA are shown for temperature changes and physical activity of HRF-2CA vs. PBS (red) in WT mice or HRF-C172A vs WT mice (green).

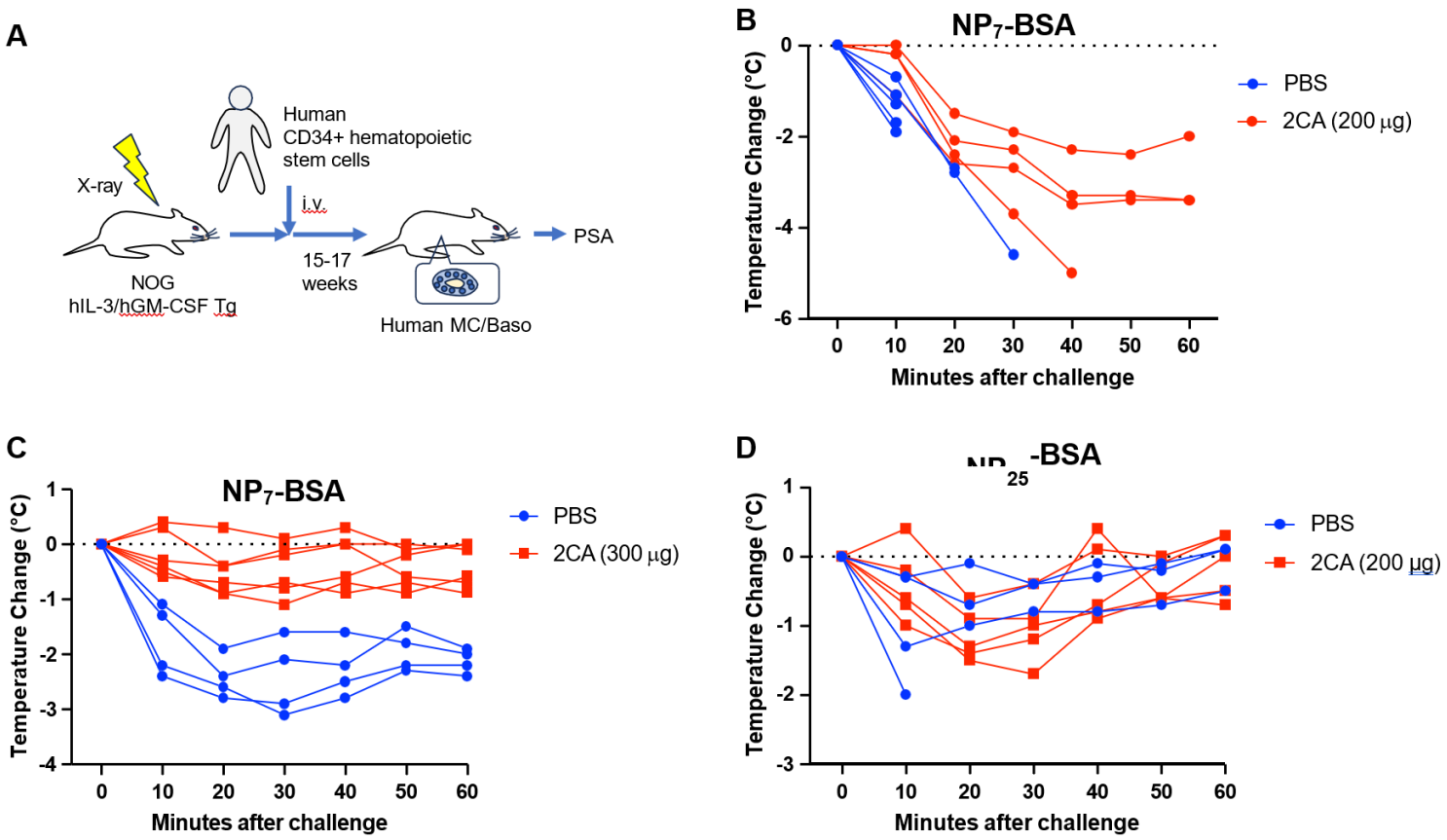

Figure 7: HRF-2CA protects from intermediate-valency antigen-induced PSA in humanized mice. (A) Experimental scheme. (B-D) PSA experiments were performed with humanized NOG hIL3/hGM mice by passive i.v. sensitization with NP-specific human IgE (1.6 μg) and challenged next day with NP_7-BSA or NP_{25}-BSA (500 μg, i.v.). 30 min before antigen challenge, mice received oral PBS or HRF-2CA (200 μg in B & D; 300 μg in C). Body temperature and deaths of individual mice were monitored.

Discussion

The present study demonstrates that HRF multimers enhance degranulation and cytokine production in IgE/antigen-induced activation of mast cells. This newly recognized function of HRF multimers enhances the sensitivity of FcεRI-expressing mast cells by lowering the antigen threshold for activation of mast cells. This is likely enabled by crosslinking HRF-reactive IgE-FcεRI complexes by HRF multimers. High avidity of HRF multimers that bind to IgE/FcεRI complexes will also contribute to mast cell activation. Although HRF dimers could enhance antigen/IgE-induced cytokine production, their effects in real life may be transient as they will be quickly converted to higher-molecular-weight multimers outside the cell and represent vanishingly small fractions compared with higher-molecular-weight multimers in nasal washes, saliva and tears from healthy individuals or in nasal washes from rhinovirus-infected asthmatic individuals [20,21]. Interestingly, there are predominant sizes of HRF multimers depending on the tissues or culture supernatants of cells (e.g., ~150 kDa and two bands of >250 kDa in nasal washes), although purified HRF proteins in an aqueous solution exhibit a ladder of many different sizes on SDS-PAGE [20]. It may be interesting to pursue their activity of these main HRF complexes in *in-vitro* mast cell activation and in gastrointestinal and respiratory tracts in relation with food allergy and asthma, respectively.

The HRF-dependent lowered threshold for activation is not antigen-specific but rather semi-ubiquitous in the requirement of antigen specificity, as a substantial subset (~30%) of IgE antibodies with different antigen specificities can be recognized by HRF and HRF-2CA inhibited *In-vivo* allergic responses initiated by using TNP-BSA (Figs. 4, 5), OVA (Fig. 6) and NP (Fig. 7) as antigens [22]. As a basis for its broad antigen reactivity, HRF-reactive antibodies include germline or quasi-germline encoded seemingly natural antibodies, as well as relevant antigen-driven or irrelevant antigen-driven antibodies with SHM. Some high-affinity HRF-reactive IgG1 antibodies such as B-G7 and D-G10 may be considered HRF-specific, as they have properties in common with anti-N19 mAb F7-1, i.e., the presence of multiple mutations in their VH and VL domains likely generated by SHM and their predicted

interactions with the N19 region of HRF. Type 2 immunity underlying allergies creates epithelial and mucosal tissue conditions rich in IL-4, IL-5, IL-9, IL-13 and other cytokines, where anaphylactic high-affinity IgE antibodies are generated by class switch recombination from IgM through IgG1 to IgE [24,51-53]. HRF-specific IgG1 antibodies such as B-G7 and D-G10 will be converted to anti-HRF IgE. In such tissues, mast cells can be easily activated by antigen; in addition to HRF multimers-mediated formation of IgE/FcεRI complexes, simultaneous exposure to antigen will increase the number of crosslinked FcεRI complexes by antigen-specific IgE (plus anti-HRF IgE), eventually reaching the activation threshold [54]. As various stimuli and situations including cell deaths and their by-products (e.g., ATP and adenosine) cause HRF release, viral, bacterial and parasitic infections as well as other inflammatory conditions causing cell deaths might also involve HRF-mediated promotion of mast cell activation [20,21].

HRF/TCTP is one of the most abundant proteins expressed by most cell types. Its intracellular functions are so fundamental to animal development that knockouts of this gene in mice lead to an early embryonic lethality [55,56]. Similar lethal fate of the gene knockout was also observed in Drosophila [57]. In addition to functions in development and other physiological processes, our study suggests that HRF proteins secreted or released by tissue injury may serve as an alarmin with which to render mast cells highly sensitive and responsive to minute amounts of antigen. This possibility is plausible, as natural IgE, antigen-irrelevant IgE and antigen-relevant IgE molecules can interact with HRF. IgE and mast cells play a critical role in the host defense against insults by venoms, toxins, environmental irritants, bacteria, viruses and helminths [58-60]. Thus, HRF may serve as an intracellular survival and proliferative factor as well as as an extracellular alarmin or a damage-associated molecular pattern for the host defense against various insults [20]. We recently showed that HRF is secreted from human brochial epithelial cells by HDM stimulation via TLR2 and several HDM allergens use TLR2 for HRF secretion [20]. Interestingly, another study suggested that hHRF directly binds to and activates TLR2 [61]. These studies combined imply that HRF secretion induced by HDM might be regulated by a positive feedback via TLR2. Furthermore, HDM-mediated HRF secretion is strongly enhanced not only by Th2 cytokines (IL-4, IL-5, IL-13) but also by epithelial-derived (TSLP, IL-25, IL-33) and pronflammatory (IL-1β, IL-6, TNF) cytokines, despite modest effects of these individual cytokines alone on HRF secretion [20]. FcεRI and TLR2 mediate synergistic signals to markedly augment cytokine production in mast cells, although their synergistic effects on degranulation were reported by some, but not other studies [62-68]. Therefore, it will be interesting to investigate if HRF multimers influence effects of co-stimulation of FcεRI and TLR2 in mast cells.

Enhancing effects of HRF multimers on antigen/IgE-mediated mast cell activation were observed at the suboptimal antigen range. This seemed to occur during *In-vivo* allergic reactions, as mast cell activation was shown by increased MCPT1 in blood. Potentially related to the HRF function, there is a known difference in antigen dose requirement for mast cell activation, i.e., a higher antigen threshold required for degranulation than that for cytokine production/secretion [36]. This difference is underlined by the differences in intracellular signaling events leading to degranulation and cytokine production/secretion, including Gab2 and p38MAPK phosphorylation by weak stimulation favoring only cytokine production/secretion and LAT and ERK2 phosphorylation by stronger stimulation and the degranulation-inhibitory role of the cortical actin cytoskeleton [6,69-71]. The fact that only positive regulatory effects of HRF are seen in standard *In-vivo* anaphylaxis and food allergy models suggests that these *In-vivo* allergic reactions are performed under suboptimal antigen concentrations. The magnitude of allergic reactions might be influenced by the time course of HRF multimerization, which could be influenced by oxidative environment. We are not aware that the cytoplasm of mast cells is different from other cell types in its oxidoreductive state, although the content inside their secretory granules is highly oxidative. The plasma membrane and cytoplasmic compartments where the initial signaling events occur after FcεRI aggregation with IgE and antigen (plus HRF multimers) are reductive. By contrast, the environment outside the cell is highly oxidative.

Conclusion

In conclusion, HRF interacts with various Ig-Fab sequences including those of natural antibodies. Disulfide-linked multimerization of HRF proceeds non-enzymatically outside the cell. This study collectively supports the notion that, by binding to FcεRI-bound IgE molecules, HRF multimers lower the threshold of antigen amounts required for FcεRI activation and enhance the magnitude of activation of mast cells, thus triggering brisk allergic reactions. Therefore, HRF operates as an endogenous allergen-like molecule for antigen/IgE/FcεRI-mediated activation of the allergy effector cells. This study also indicates that the blockade of IgE-HRF interactions prevents allergic reactions by raising the activation threshold for antigen. Production of HRF-reactive IgE and IgG by immunization with irrelevant antigens also implies their potential pathogenic role in infection, autoimmunity and post-vaccination adverse effects.

Conflict of Interest

T.K. and Y.K. served as consultants for Escient Pharma. T.K., Y.K. and T.M. have pending or issued patents. The other authors declare no other competing interests.

Funding Statement

This research was supported in part by the U.S. National Institutes of Health grants AI46042 and AI153867, Kyowa Kirin, Inc. and Platform Project for Supporting Drug Discovery and Life Science Research (Basis for Supporting Innovative Drug Discovery and Life Science Research (BINDS)) from Japan's AMED under Grant Number JP20am0101121. Yu K. was supported by NIH grant T32AI125179 during part of this project.

Acknowledgement

This research was supported in part by the U.S. National Institutes of Health grants AI46042 and AI153867, Kyowa Kirin, Inc. and Platform Project for Supporting Drug Discovery and Life Science Research (Basis for Supporting Innovative Drug Discovery and Life Science Research (BINDS)) from Japan's AMED under Grant Number JP20am0101121. Yu K. was supported by NIH grant T32AI125179 during part of this project.

Data Availability Statement

Not applicable.

Ethical Statement

The project did not meet the definition of human subject research under the purview of the IRB according to federal regulations and therefore, was exempt.

Informed Consent Statement

Informed consent was taken for this study.

Authors' Contributions

Yu K., T.A., K.S., T.M., Y.K. and T.K. designed most experiments. Yu K., T.A., R.I., K.K., S.-W.H., G.D., R.Y., J.F., J.L., S.B., K.I., J.K. and H.K. performed experiments. T.A. and R.Y. conducted structure predictions. K.S., C.D.S., H.K. and T.M. directed part of the study. Y.K. and T.K. conceived and directed the entire project. T.K. wrote the manuscript with input from all coauthors.

References

1. Mukai K, Matsuoka K, Taya C, Suzuki H, Yokozeki H, Nishioka K, et al. Basophils play a critical role in the development of IgE-mediated chronic allergic inflammation independently of T cells and mast cells. Immunity. 2005;23(2):191-202.
2. Gould HJ, Sutton BJ, Beavil AJ, Beavil RL, McCloskey N, Coker HA, et al. The biology of IgE and the basis of allergic disease. Annu Rev Immunol. 2003;21:579-628.
3. Turner H, Kinet JP. Signalling through the high-affinity IgE receptor Fc epsilonRI. Nature. 1999;402(6760 Suppl):B24-30.
4. Gould HJ, Wu YB. IgE repertoire and immunological memory: compartmental regulation and antibody function. Int Immunol. 2018;30(9):403-12.
5. Fewtrell C, Metzger H. Larger oligomers of IgE are more effective than dimers in stimulating rat basophilic leukemia cells. J Immunol. 1980;125(2):701-10.
6. Gonzalez-Espinosa C, Odom S, Olivera A, Hobson JP, Martinez ME, Oliveira-Dos-Santos A, et al. Preferential signaling and induction of allergy-promoting lymphokines upon weak stimulation of the high affinity IgE receptor on mast cells. J Exp Med. 2003;197(11):1453-65.
7. Pali-Scholl I, Jensen-Jarolim E. The concept of allergen-associated molecular patterns (AAMP). Curr Opin Immunol. 2016;42:113-8.
8. McCoy KD, Harris NL, Diener P, Hatak S, Odermatt B, Hangartner L, et al. Natural IgE production in the absence of MHC Class II cognate help. Immunity. 2006;24(3):329-39.
9. Crawford G, Hayes MD, Seoane RC, Ward S, Dalessandri T, Lai C, et al. Epithelial damage and tissue gammadelta T cells promote a unique tumor-protective IgE response. Nat Immunol. 2018;19(8):859-70.

10. Hayes MD, Ward S, Crawford G, Seoane RC, Jackson WD, Kipling D, et al. Inflammation-induced IgE promotes epithelial hyperplasia and tumour growth. Elife. 2020;9.
11. Asai K, Kitaura J, Kawakami Y, Yamagata N, Tsai M, Carbone DP, et al. Regulation of mast cell survival by IgE. Immunity. 2001;14(6):791-800.
12. Kalesnikoff J, Huber M, Lam V, Damen JE, Zhang J, Siraganian RP, et al. Monomeric IgE stimulates signaling pathways in mast cells that lead to cytokine production and cell survival. Immunity. 2001;14(6):801-11.
13. Furuichi K, Rivera J, Triche T, Isersky C. The fate of IgE bound to rat basophilic leukemia cells. IV. Functional association between the receptors for IgE. J Immunol. 1985;134(3):1766-73.
14. Yamaguchi M, Lantz CS, Oettgen HC, Katona IM, Fleming T, Miyajima I, et al. IgE enhances mouse mast cell Fc(epsilon)RI expression *in-vitro* and *in-vivo*: evidence for a novel amplification mechanism in IgE-dependent reactions. J Exp Med. 1997;185(4):663-72.
15. Lim J, Lin EV, Hong JY, Vaidyanathan B, Erickson SA, Annicelli C, et al. Induction of natural IgE by glucocorticoids. J Exp Med. 2022;219(10).
16. Bommer UA. Cellular function and regulation of the translationally controlled tumor protein TCTP. Open Allergy J. 2012;5:19-32.
17. Bommer UA, Thiele BJ. The translationally controlled tumour protein (TCTP). Int J Biochem Cell Biol. 2004;36(3):379-385.
18. MacDonald SM. Histamine releasing factors and IgE heterogeneity. In: Middleton E, Reed CE, Ellis EF, Adkinson NF, Yunginger JW, Busse WW, editors. St. Louis, Missouri: Mosby-Year Book Incorporated. 1993.
19. Yoneda K, Rokutan K, Nakamura Y, Yanagawa H, Kondo-Teshima S, Sone S. Stimulation of human bronchial epithelial cells by IgE-dependent histamine-releasing factor. Am J Physiol Lung Cell Mol Physiol. 2004;286(1):L174-181.
20. Kasakura K, Kawakami Y, Jacquet A, Kawakami T. Histamine-releasing factor is a novel alarmin induced by house dust mite allergen, cytokines and cell death. J Immunol. 2022;209(10):1851-9.
21. Kawakami Y, Takazawa I, Fajt ML, Kasakura K, Lin J, Ferrer J, et al. Histamine-releasing factor in severe asthma and rhinovirus-associated asthma exacerbation. J Allergy Clin Immunol. 2023.
22. Kashiwakura JC, Ando T, Matsumoto K, Kimura M, Kitaura J, Matho MH, et al. Histamine-releasing factor has a proinflammatory role in mouse models of asthma and allergy. J Clin Invest. 2012;122(1):218-28.
23. Ando T, Kashiwakura JI, Itoh-Nagato N, Yamashita H, Baba M, Kawakami Y, et al. Histamine-releasing factor enhances food allergy. J Clin Invest. 2017;127(12):4541-53.
24. Kawakami Y, Kurosawa Y, Oltean D, Espinosa LY, Kim HS, Lemersal I, et al. Novel inhibitors of histamine-releasing factor suppress food allergy in a murine model. Allergol Int. 2022;71(1):147-9.
25. Dore KA, Kashiwakura JI, McDonnell JM, Gould HJ, Kawakami T, Sutton BJ, et al. Crystal structures of murine and human histamine-releasing factor (HRF/TCTP) and a model for HRF dimerisation in mast cell activation. Mol Immunol. 2018;93:216-22.
26. Kim M, Min HJ, Won HY, Park H, Lee JC, Park HW, et al. Dimerization of translationally controlled tumor protein is essential for its cytokine-like activity. PLoS One. 2009;4(7):e6464.
27. Huang X, Li Z, Sun R. Synergistic actions of histamine-releasing factor and histamine-releasing factor-reactive IgE in chronic urticaria. Int Arch Allergy Immunol. 2017;172(1):27-32.
28. Hong SW, O E, Lee JY, Lee M, Han D, Ko HJ, et al. Food antigens drive spontaneous IgE elevation in the absence of commensal microbiota. Sci Adv. 2019;5(5):eaaw1507.
29. Kim KS, Hong SW, Han D, Yi J, Jung J, Yang BG, et al. Dietary antigens limit mucosal immunity by inducing regulatory T cells in the small intestine. Science. 2016;351(6275):858-63.
30. Holodick NE, Rodriguez-Zhurbenko N, Hernandez AM. Defining natural antibodies. Front Immunol. 2017;8:872.
31. Panda S, Ding JL. Natural antibodies bridge innate and adaptive immunity. J Immunol. 2015;194(1):13-20.
32. Reyneveld GI, Savelkoul HFJ, Parmentier HK. Current understanding of natural antibodies and exploring the possibilities of modulation using veterinary models: a review. Front Immunol. 2020;11:2139.
33. Smith SA, Chruszcz M, Chapman MD, Pomes A. Human monoclonal IgE antibodies - a major milestone in allergy. Curr Allergy Asthma Rep. 2023;23(1):53-65.
34. Go YM, Jones DP. Redox compartmentalization in eukaryotic cells. Biochim Biophys Acta. 2008;1780(11):1273-90.
35. Lopez-Mirabal HR, Winther JR. Redox characteristics of the eukaryotic cytosol. Biochim Biophys Acta. 2008;1783(4):629-40.
36. Xiao W, Nishimoto H, Hong H, Kitaura J, Nunomura S, Maeda-Yamamoto M, et al. Positive and negative regulation of mast

cell activation by Lyn via the Fc epsilonRI. J Immunol. 2005;175(10):6885-92.
37. McNeil BD, Pundir P, Meeker S, Han L, Undem BJ, Kulka M, et al. Identification of a mast-cell-specific receptor crucial for pseudo-allergic drug reactions. Nature. 2015;519(7542):237-41.
38. Susini L, Besse S, Duflaut D, Lespagnol A, Beekman C, Fiucci G, et al. TCTP protects from apoptotic cell death by antagonizing bax function. Cell Death Differ. 2008;15(8):1211-20.
39. Jumper J, Evans R, Pritzel A, Green T, Figurnov M, Ronneberger O, et al. Highly accurate protein structure prediction with AlphaFold. Nature. 2021;596(7873):583-9.
40. Tunyasuvunakool K, Adler J, Wu Z, Green T, Zielinski M, Zidek A, et al. Highly accurate protein structure prediction for the human proteome. Nature. 2021;596(7873):590-6.
41. Mirdita M, Schutze K, Moriwaki Y, Heo L, Ovchinnikov S, Steinegger M. ColabFold: making protein folding accessible to all. Nat Methods. 2022;19(6):679-82.
42. Lee H, Kim MS, Lee JS, Cho H, Park J, Shin DH, et al. Flexible loop and helix 2 domains of TCTP are the functional domains of dimerized TCTP. Sci Rep. 2020;10(1):197.
43. Dombrowicz D, Flamand V, Brigman KK, Koller BH, Kinet JP. Abolition of anaphylaxis by targeted disruption of the high affinity immunoglobulin E receptor alpha chain gene. Cell. 1993;75(5):969-76.
44. Finkelman FD. Anaphylaxis: lessons from mouse models. J Allergy Clin Immunol. 2007;120(3):506-15.
45. Tauber M, Basso L, Martin J, Bostan L, Pinto MM, Thierry GR, et al. Landscape of mast cell populations across organs in mice and humans. J Exp Med. 2023;220(10).
46. Sindher SB, Long A, Chin AR, Hy A, Sampath V, Nadeau KC, et al. Food allergy, mechanisms, diagnosis and treatment: innovation through a multi-targeted approach. Allergy. 2022;77(10):2937-48.
47. Yu W, Freeland DMH, Nadeau KC. Food allergy: immune mechanisms, diagnosis and immunotherapy. Nat Rev Immunol. 2016;16(12):751-65.
48. Brandt EB, Strait RT, Hershko D, Wang Q, Muntel EE, Scribner TA, et al. Mast cells are required for experimental oral allergen-induced diarrhea. J Clin Invest. 2003;112(11):1666-77.
49. Ito R, Takahashi T, Katano I, Kawai K, Kamisako T, Ogura T, et al. Establishment of a human allergy model using human IL-3/GM-CSF-transgenic NOG mice. J Immunol. 2013;191(6):2890-99.
50. Hakimi J, Seals C, Kondas JA, Pettine L, Danho W, Kochan J. The alpha subunit of the human IgE receptor (FcERI) is sufficient for high affinity IgE binding. J Biol Chem. 1990;265(36):22079-81.
51. Lambrecht BN, Hammad H, Fahy JV. The cytokines of asthma. Immunity. 2019;50(4):975-91.
52. Lloyd CM, Snelgrove RJ. Type 2 immunity: expanding our view. Sci Immunol. 2018;3(25).
53. Xiong H, Dolpady J, Wabl M, Curotto de Lafaille MA, Lafaille JJ. Sequential class switching is required for the generation of high affinity IgE antibodies. J Exp Med. 2012;209(2):353-64.
54. Hjort C, Schiotz PO, Ohlin M, Wurtzen PA, Christensen LH, Hoffmann HJ. The number and affinity of productive IgE pairs determine allergen activation of mast cells. J Allergy Clin Immunol. 2017;140(4):1167-70.
55. Chen SH, Wu PS, Chou CH, Yan YT, Liu H, Weng SY, et al. A knockout mouse approach reveals that TCTP functions as an essential factor for cell proliferation and survival in a tissue- or cell type-specific manner. Mol Biol Cell. 2007;18(7):2525-32.
56. Koide Y, Kiyota T, Tonganunt M, Pinkaew D, Liu Z, Kato Y, et al. Embryonic lethality of fortilin-null mutant mice by BMP-pathway overactivation. Biochim Biophys Acta. 2009;1790(5):326-38.
57. Hsu YC, Chern JJ, Cai Y, Liu M, Choi KW. Drosophila TCTP is essential for growth and proliferation through regulation of dRheb GTPase. Nature. 2007;445(7129):785-8.
58. Dudeck A, Koberle M, Goldmann O, Meyer N, Dudeck J, Lemmens S, et al. Mast cells as protectors of health. J Allergy Clin Immunol. 2019;144(4 Suppl):S4-18.
59. Mukai K, Tsai M, Starkl P, Marichal T, Galli SJ. IgE and mast cells in host defense against parasites and venoms. Semin Immunopathol. 2016;38(5):581-603.
60. Palm NW, Rosenstein RK, Medzhitov R. Allergic host defences. Nature. 2012;484(7395):465-72.
61. Hangai S, Kawamura T, Kimura Y, Chang CY, Hibino S, Yamamoto D, et al. Orchestration of myeloid-derived suppressor cells in the tumor microenvironment by ubiquitous cellular protein TCTP released by tumor cells. Nat Immunol. 2021;22(8):947-57.
62. Qiao H, Andrade MV, Lisboa FA, Morgan K, Beaven MA. Fc epsilonR1 and toll-like receptors mediate synergistic signals to markedly augment production of inflammatory cytokines in murine mast cells. Blood. 2006;107(2):610-8.

63. Supajatura V, Ushio H, Nakao A, Akira S, Okumura K, Ra C, et al. Differential responses of mast cell toll-like receptors 2 and 4 in allergy and innate immunity. J Clin Invest. 2002;109(10):1351-9.
64. Varadaradjalou S, Feger F, Thieblemont N, Hamouda NB, Pleau JM, Dy M, et al. Toll-like receptor 2 (TLR2) and TLR4 differentially activate human mast cells. Eur J Immunol. 2003;33(4):899-906.
65. McCurdy JD, Olynych TJ, Maher LH, Marshall JS. Cutting edge: distinct Toll-like receptor 2 activators selectively induce different classes of mediator production from human mast cells. J Immunol. 2003;170(4):1625-9.
66. Ikeda T, Funaba M. Altered function of murine mast cells in response to lipopolysaccharide and peptidoglycan. Immunol Lett. 2003;88(1):21-6.
67. Matsushima H, Yamada N, Matsue H, Shimada S. TLR3-, TLR7- and TLR9-mediated production of proinflammatory cytokines and chemokines from murine connective tissue-type skin-derived mast cells but not from bone marrow-derived mast cells. J Immunol. 2004;173(1):531-41.
68. Mrabet-Dahbi S, Metz M, Dudeck A, Zuberbier T, Maurer M. Murine mast cells secrete a unique profile of cytokines and prostaglandins in response to distinct TLR2 ligands. Exp Dermatol. 2009;18(5):437-44.
69. Foger N, Jenckel A, Orinska Z, Lee KH, Chan AC, Bulfone-Paus S. Differential regulation of mast cell degranulation versus cytokine secretion by the actin regulatory proteins Coronin1a and Coronin1b. J Exp Med. 2011;208(9):1777-87.
70. Frigeri L, Apgar JR. The role of actin microfilaments in the down-regulation of the degranulation response in RBL-2H3 mast cells. J Immunol. 1999;162(4):2243-50.
71. Nishida K, Yamasaki S, Ito Y, Kabu K, Hattori K, Tezuka T, et al. Fc epsilonRI-mediated mast cell degranulation requires calcium-independent microtubule-dependent translocation of granules to the plasma membrane. J Cell Biol. 2005;170(1):115-26.

Supplementary Information

Well #	Jurkat	non-B	B	HRF	Insulin	IgM
A1	(-)	(-)	(-)	(-)	(-)	(+)
A2	(-)	(-)	(-)	(+/-)	(-)	(+)
A3	(-)	(+)	(-)	(-)	(-)	(++)
A4	(-)	(-)	(-)	(+/-)	(-)	(++)
A5	(-)	(-)	(-)	(-)	(-)	(+)
A6	(-)	(+)	(+)	(+/-)	(-)	(+)
A7	(-)	(+)	(-)	(-)	(-)	(+)
A8	(+)	(+/-)	(-)	(-)	(-)	(+)
A9	(-)	(-)	(-)	(++)	(++)	(+++)
A10	(-)	(-)	(-)	(-)	(-)	(+)
A11	(-)	(+)	(+)	(+/-)	(-)	(+++)
A12	(-)	(+)	(+)	(+)	(-)	(++)
B1	(-)	(-)	(-)	(-)	(+/-)	(++)
B2	(-)	(-)	(-)	(++)	(++)	(+++)
B3	(-)	(-)	(-)	(++)	(+)	(++)
B4	(-)	(-)	(-)	(+)	(++)	(+++)
B5	(-)	(p+)	(-)	(-)	(-)	(+)
B6	(-)	(-)	(-)	(-)	(-)	(+)
B7	(-)	(-)	(-)	(+/-)	(-)	(+)
B8	(-)	(+)	(+)	(-)	(-)	(+)
B9	(-)	(-)	(-)	(-)	(-)	(+)
B10	(-)	(-)	(-)	(+/-)	(-)	(+/-)
B11	(-)	(-)	(-)	(-)	(-)	(+)
B12	(-)	(-)	(-)	(-)	(-)	(+)
C1	(-)	(-)	(-)	(-)	(-)	(+)
C2	(-)	(+/-)	(+)	(+/-)	(-)	(+)
C3	(-)	(-)	(-)	(-)	(-)	(++)
C4	(-)	(-)	(-)	(+/-)	(-)	(++)
C5	(-)	(-)	(-)	(-)	(-)	(+)
C6	(-)	(-)	(-)	(-)	(-)	(+)
C7	(-)	(-)	(-)	(-)	(-)	(+/-)
C8	(-)	(-)	(-)	(-)	(-)	(+)
C9	(-)	(-)	(-)	(-)	(-)	(+)
C10	(-)	(-)	(-)	(++)	(++)	(+++)
C11	(-)	(-)	(-)	(++)	(+/-)	(++)
C12	(p+)	(p+)	(-)	(+/-)	(+/-)	(+)
D1	(-)	(+)	(+)	(-)	(-)	(+/-)
D2	(-)	(p+)	(+)	(++)	(-)	(+/-)
D3	(-)	(-)	(-)	(-)	(+/-)	(+)
D4	(-)	(+)	(+)	(-)	(-)	(+)
D5	(-)	(-)	(-)	(-)	(-)	(+)
D6	(-)	(-)	(-)	(-)	(-)	(+/-)
D7	(-)	(-)	(-)	(-)	(-)	(+)
D8	(-)	(-)	(-)	(-)	(-)	(++)
D9	(+)	(-)	(-)	(+/-)	(++)	(+++)

D10	(-)	(-)	(-)	(+)	(-)	(++)
D11	(-)	(-)	(-)	(-)	(-)	(+/-)
D12	(-)	(-)	(-)	(-)	(-)	(+)
E1	(-)	(-)	(-)	(-)	(-)	(+)
E2	(-)	(-)	(-)	(-)	(-)	(+)
E3	(-)	(-)	(-)	(-)	(+)	(+)
E4	(-)	(-)	(-)	(-)	(+/-)	(+++)
E5	(-)	(-)	(-)	(+)	(+/-)	(+++)
E6	(-)	(+)	(+)	(-)	(-)	lo
E7	(-)	(+)	(+)	(-)	(-)	(+)
E8	(-)	(-)	(-)	(-)	(-)	(+)
E9	(-)	(-)	(-)	(-)	(-)	(+/-)
E10	(-)	(-)	(-)	(-)	(-)	(+)
E11	(-)	(-)	(-)	(-)	(-)	(++)
E12	(++)	(+)	(-)	(++)	(+)	(++)
F1	(-)	(-)	(-)	(-)	(-)	(+)
F2	(-)	(-)	(-)	(-)	(-)	(++)
F3	(-)	(-)	(-)	(-)	(-)	lo
F4	(-)	(p+)	(+)	(-)	(-)	lo
F5	(-)	(-)	(-)	(-)	(-)	(++)
F6	(-)	(-)	(-)	(-)	(+)	(++)
F7	(-)	(-)	(-)	(-)	(-)	(+)
F8	(+)	(-)	(-)	(-)	(-)	(+)
F9	(-)	(-)	(-)	(+)	(+)	(++)
F10	(-)	(-)	(-)	(+/-)	(-)	(+)
F11	(-)	(p+)	(-)	(-)	(++)	(+++)
F12	(-)	(-)	(-)	(++)	(++)	(+++)
G1	(-)	(p+)	(+)?	(-)	(-)	(+/-)
G2	(-)	(-)	(-)	(-)	(-)	(+)
G3	(-)	(p+)	(-)	(-)	(+/++)	(++)
G4	(-)	(-)	(-)	(-)	(-)	(+)
G5	(+)	(-)	(-)	(-)	(-)	(+)
G6	(-)	(-)	(-)	(-)	(-)	(+/-)
G7	(-)	(-)	(-)	(-)	(-)	(+/-)
G8	(-)	(-)	(-)	(+/-)	(-)	(++)
G9	(-)	(-)	(+)	(-)	(-)	(+/-)
G10	(-)	(+)	(+)	(-)	(-)	(+/-)
G11	(-)	(-)	(-)	(-)	(-)	(+/++)
G12	(-)	(-)	(-)	(-)	(-)	(+)
H1	(-)	(-)	(-)	(-)	(-)	(+/-)
H2	(p+)	(p+)	(-)	(-)	(-)	(++)
H3	(-)	(-)	(-)	(-)	(-)	(+)
H4	(-)	(-)	(-)	(++)	(+)	(++)
H5	(+)	(p+)	(-)	(-)	(-)	lo
H6	(-)	(-)	(-)	(-)	(-)	(+)
H7	(+)	(+)	(+)	(-)	(-)	(+)
H8	(-)	(-)	(+)	(+/-)	(-)	(+/-)
H9	(-)	(-)	(-)	(-)	(-)	(+/-)

H10	(-)	(-)	(-)	(+/-)	(++)	(+++)
H11	(-)	(-)	(-)	(-)	(-)	(+)
H12	(-)	(-)	(-)	(-)	(-)	(+/-)
IgM molecules derived from 96 different EBV-transformed cord blood B cell cultures were tested for their reactivities with HRF, insulin and cell surface components of adult blood mononuclear cells and GFP(+) Jurkat cell mixtures. IgM clones reactive with HRF and insulin are highlighted in yellow.						

Table S1: Polyreactivity of human cord blood B cell-derived IgM molecules.

Clone	IGHV	Cluster	HCDR3	LCDR3	HRF binding*
D-C2	EM72	1a	ARFGTD	LQHLNYPLT	15.8
A-F3	EM72	1b	ARFGTD	LQHLNYPLT	2.9
D-G10	EM72	2a	TSYAMDY	LQHWNYPLT	57.7
A-C5	EM72	2a	TSYAMDY	LQHWNYPLT	17.8
R4A-H10	EM72	2a	TSYAMDY	LQHWNYPLT	3.5
D-F9	EM72	2b	TSYAMDY	LQHWNYPLT	52.2
R4A-H8	EM72	2c	TSYAMDY	LQHWNYPYT	8.1
R4B-H10	EM72	2c	TSYAMDY	LQHWNYPYT	28.4
B-G7	WECQ	3a	ATGLAY	QQHYSTPWT	62.1
A-E12	WECQ	3b	ATGLAY	QQHYSTPFT	34.4
D-A1	WECQ	3c	ATGLAY	QQYSSYPFT	9.6
B-G12	WECQ	3d	ATGLAY	QQYSSFPLT	48.4
D-B5	WECQ	3d	ATGLAY	QQYSSFPLT	46.5
B-E3	WECQ	3d	ATGLAY	QQYSSFPLT	11.3
B-G11	WECQ	3d	ATGLAY	QQYSSFPLT	0.8
C-B3	WECQ	3e	ATGLAY	QQHYSTP-T	37.5
R4B-D12	WECQ	3f	ATGLAY	QQYSSFPLT	4.0
R4B-G1	WECQ	3g	ATGLAY	QQYNNFPFT	10.8
C-G3	2CAX	3h	ATGLAY	QQGITLPWT	7.6
B-E10	MUFD	4	ARYIGGSSPFDY	QQGITLPWT	11.1
A-B11	MUFD	5	ARAGAMDY	SQSTHVPPWT	12.3
D-B4	PCIZ	6	ARYGWAFDY	QQYSSYPYT	2.2
C-G9	PCIZ	6	ARYGWAFDY	QQYGSYPLT	1.2
A-A3	D4D7	7	ARNWDYFDY	QQGNTLPRT	2.3
D-A10	EM72	8	LTGDY	LQHWNYPLT	23.6
C-G8	EM72	8	LTGDY	LQHWNYPLT	13.1
C-H7	EM72	8	LTGDY	LQHWNYPLT	10.9
R4B-A4	EM72	8	LTGDY	LQHWNYPLT	1.6
R4B-A6	EM72	8	LTGDY	LQHWNYPLT	1.5
R4B-D1	EM72	8	LTGDY	LQHWNYPLT	0.6
R4B-E11	EM72	8	LTGDY	LQHWNYPLT	1.2
R4B-H4	EM72	8	LTGDY	LQHWNYPLT	2.3
D-G3	2CAX	9	AREGSYRRPMDY	LQHWNYPFT	1.1
D-A11	5UXG	10	ARSTALYDYSY	QHSREFPWTF	2.1
A-C9	LALY	11	RGWDY	QQWSSNPPT	15.3
A-H2	3F5C	12	ARREGYGNYFYYAMDY	QHSRELRT	11.4
A-G8	VCP7	13	ARYGNGFYFFPY	QQYWDTPFT	13.3
Phage display libraries generated from spleen cells of mice immunized with L-SIGN/Fc, DC-SIGN/Fc, CD80/Fc-His, CD86/Fc-His and bacterial LPS were screened by panning for reactivity to plate-bound mHRF. Isolated HRF-reactive IgG1						

molecules were sequenced. *Relative HRF binding ability was calculated by dividing the OD450 nm value of a phage clone binding to mHRF-His by that of the same phage clone binding to CD80/Fc-His.

Table S2: HRF-reactive IgG1 molecules derived from mice immunized with irrelevant antigens.

Clone	Cluster	IGHV	IGHJ	# mutations*
D-C2	1a	EM72	J2	12 + 6
A-F3	1b	EM72	J2	12 + 6
D-G10	2a	EM72	J4	15 + 4
A-C5	2a	EM72	J4	15 + 4
R4A-H10	2a	EM72	J4	15 + 4
D-F9	2b	EM72	J4	15 + 4
R4A-H8	2c	EM72	J4	16 + 4
R4B-H10	2c	EM72	J4	16 + 4
B-G7	3a	WECQ	J3	3 + 1
A-E12	3b	WECQ	J3	3 + 2
D-A1	3c	WECQ	J3	2 + 3
B-G12	3d	WECQ	J3	7 + 6
D-B5	3d	WECQ	J3	7 + 6
B-E3	3d	WECQ	J3	7 + 6
B-G11	3d	WECQ	J3	7 + 6
C-B3	3e	WECQ	J3	5 + 5
R4B-D12	3f	WECQ	J3	7 + 6
R4B-G1	3g	WECQ	J3	6 + 3
C-G3	3h	2CAX	J3	0 + 1
B-E10	4	EM72	J2	4 + 1
A-B11	5	MUFD	J4	7 + 5
D-B4	6	PCIZ	J2	3 + 0
C-G9	6	PCIZ	J2	2 + 0
A-A3	7	D4D7	J2	7 + 2
D-A10	8	EM72	J2	5 + 3
C-G8	8	EM72	J2	5 + 3
C-H7	8	EM72	J2	5 + 3
R4B-A4	8	EM72	J2	5 + 3
R4B-A6	8	EM72	J2	5 + 3
R4B-D1	8	EM72	J2	5 + 3
R4B-E11	8	EM72	J2	5 + 3
R4B-H4	8	EM72	J2	5 + 3
D-G3	9	2CAX	J4	2 + 3
D-A11	10	5UXG	J3	11 + 8
A-C9	11	LALY	J2	0 + 1
A-H2	12	3F5C	J4	1 + 0
A-G8	13	VCP7	J3	10 + 2

Table S3: Mutations in heavy chain V_H-(D)-J_H sequences of HRF-reactive IgG1 molecules from mice immunized with irrelevant antigens.

						V_H and V_L		V_H and mHRF/N19		V_L and mHRF/N19		V_H-interfacing a.a. in N19	V_L-interfacing a.a. in N19	Comment
						interface	ΔiG	interface	ΔiG	interface	ΔiG			
Target	V-region	Rank	pLDDT	pTM	ipTM	area, Å2	kcal/mol	area, Å2	kcal/mol	area, Å2	kcal/mol			
mHRF	B-G7	1	85.1	0.656	0.531	698	-9.9	498	-4.1	417	-1.7	1,2,4,16-19	2,5,7,10	Fig. S6D
		2	82.6	0.616	0.484	712	-11.2	636	-6.0	354	-2.6	2,7,10	-	
		3	81.2	0.612	0.478	685	-10.2	567	-5.2	350	-3.0	1-3,5,10,12,15-17	1,2,16-19	
		4	82.7	0.607	0.470	620	-7.8	557	-3.6	445	-4.8	1,3,5,10,12	1,2,4,16-19	
		5	74.4	0.432	0.408	1950	-26.2	454	-3.9	527	-3.9	2,7,8,10	1,2,4,16-19	Compromised
	D-G10	1	89.1	0.798	0.733	611	-9.0	391	-1.5	582	-1.5	1,2,16-19	2,4,7	Fig. S6D
		2	84.4	0.662	0.550	614	-9.3	392	-1.7	557	-1.8	1,2,16-19	2,4,7	
		3	83.8	0.624	0.494	602	-9.4	593	-4.3	460	-0.9	-	-	
		4	84.2	0.618	0.488	620	-8.3	523	-0.8	455	-0.8	-	-	
		5	83.6	0.617	0.479	657	-7.3	468	-0.6	685	-2.5	1,2,4,16-19	19	
	SPE-7 (non-reactive)	1	86.8	0.662	0.542	853	-13.9	612	-6.2	129	1.6	-	-	Fig. S6D
		2	86.6	0.629	0.499	868	-13.4	508	-4.1	229	1.5	-	-	
		3	85.6	0.618	0.480	853	-13.7	686	-6.6	269	0.2	-	-	
		4	83.6	0.607	0.471	883	-11.9	707	-6.9	237	0.2	-	-	
		5	84.5	0.606	0.467	862	-13.4	667	-4.0	350	-0.6	-	-	
GST-N19	F7-1	1	89.5	0.581	0.856	806	-9.2	879	-3.4	527	-4.5	1-8,12,13,15-17	2,5,10,13,14,17,18	Fig. S6E
		2	89.9	0.573	0.853	801	-9.1	895	-3.7	540	-4.7	1-8,12,13,15-17	2,5,10,13,14,17,18	
		3	88.9	0.576	0.844	799	-8.6	850	-3.0	459	-3.6	1-8,12,13-16	2,5,10,13,14,17,18	
		4	89.3	0.562	0.838	783	-8.2	864	-5.7	618	-3.6	1-8,10,12-14,16,17	2,5,10,11,14,15,17,18	
		5	86.1	0.546	0.414	800	-8.7	774	4.3	135	1.9	-	-	
	SPE-7 (non-reactive)	1	85.3	0.552	0.423	843	-13.7	720	-6.4	127	0.3	-	-	Fig. S6E
		2	86.6	0.551	0.422	876	-13.1	670	-3.9	200	-0.9	-	-	
		3	84.9	0.549	0.420	848	-12.5	640	-5.9	325	1.2	-	-	
		4	84.9	0.542	0.412	841	-11.1	513	-1.2	421	1.6	2	-	
		5	85.2	0.537	0.403	819	-11.6	495	-2.4	371	-0.1	-	-	

Five candidate structures from each AlphaFold2 multimer prediction were analyzed for the interactions between their components. The VH/VL-interfacing amino acid (a.a.) numbers are listed. pLDDT, predicted local distance difference test; pTM, predicted template modeling score; ipTM, interface pTM score.

Table S4: Predicted interactions of mHRF with high-affinity HRF-reactive IgG1s as compared with those with anti-N19 mAb F7-1 and HRF-nonreactive SPE-7 IgE.

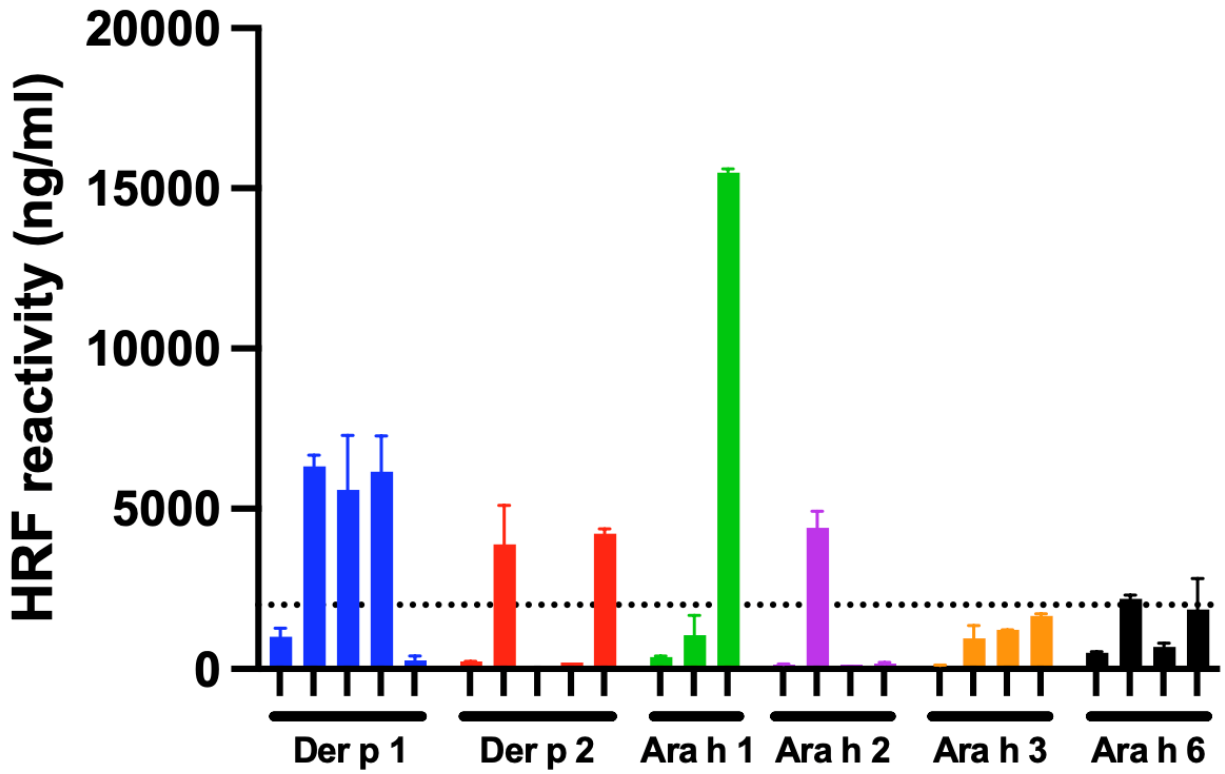

Figure S1: (Related to Fig. 1). HRF binds to a subset of peanut allergen-specific human IgE molecules. Human IgE mAbs (5 mAbs each per allergen) specific to peanut and house dust mite allergens were tested for their reactivity to hHRF by ELISA and relative reactivity was compared with the dose-response curve generated by HE-1 IgE, positive control (OD450 by 2000 ng/ml HE-1 IgE shown by a dotted line).

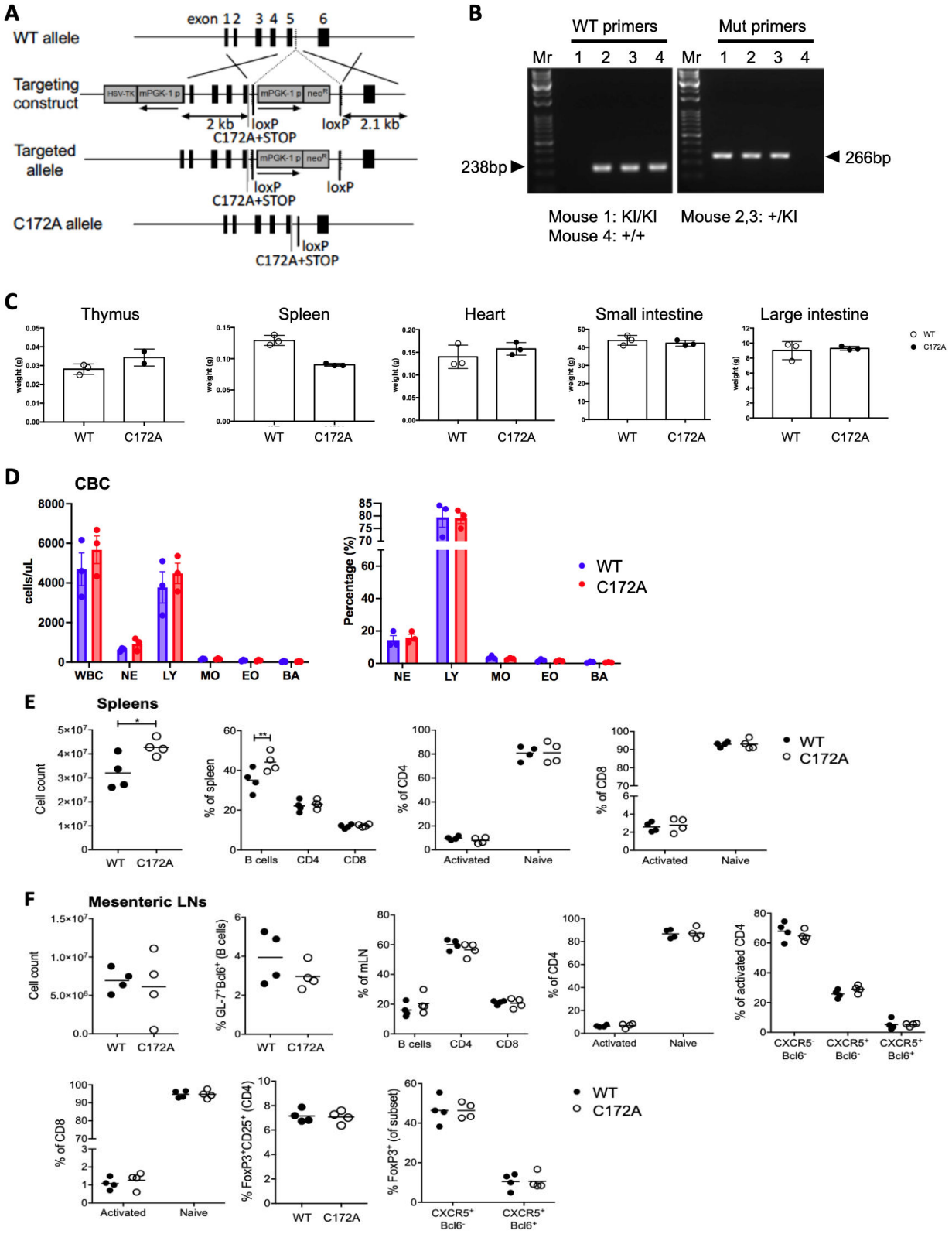

Figure S2: (Related to Figs. 2, 4, 5 and 6). Hematologic and immune phenotypes of HRF-C172A mice. (A) Scheme for the generation of HRF-C172A mice. A stop codon was introduced following the C172A codon. (B) Genotyping of four mice was performed by different PCRs encompassing both 5′ and 3′ ends of the insert followed by agarose gel analysis of their products. Shown are examples of PCR detecting the C-terminal coding region including C172A. Mouse #1 has 2 knock-in (KI) alleles; mouse #4 has 2 WT alleles; mice #2 and #3 have both WT and KI alleles. (C) Weights of major organs. (D) Complete blood count. WBC, white blood cells; NE, neutrophils; LY, lymphocytes; MO, monocytes; EO, eosinophils; BA, basophils. (E, F) Immune phenotypes of spleen cells (E) and mesenteric lymph nodes (F). Cells were quantified by flow cytometry, including

B220+ B cells, GL-7+Bcl6+ B cells, CD4+ T cells, CD8+ T cells, CD44+CD62L- activated CD4 or CD8 T cells, CD4+CD25+FoxP3+ Treg cells, CXCR5-Bcl6- activated CD4T cells, CXCR5+Bcl6- activated CD4T cells, CXCR5+Bcl6+ activated CD4 T cells, CXCR5+Bcl6-FoxP3+ CD4 T cells and CXCR5+Bcl6+FoxP3+ CD4 T cells.

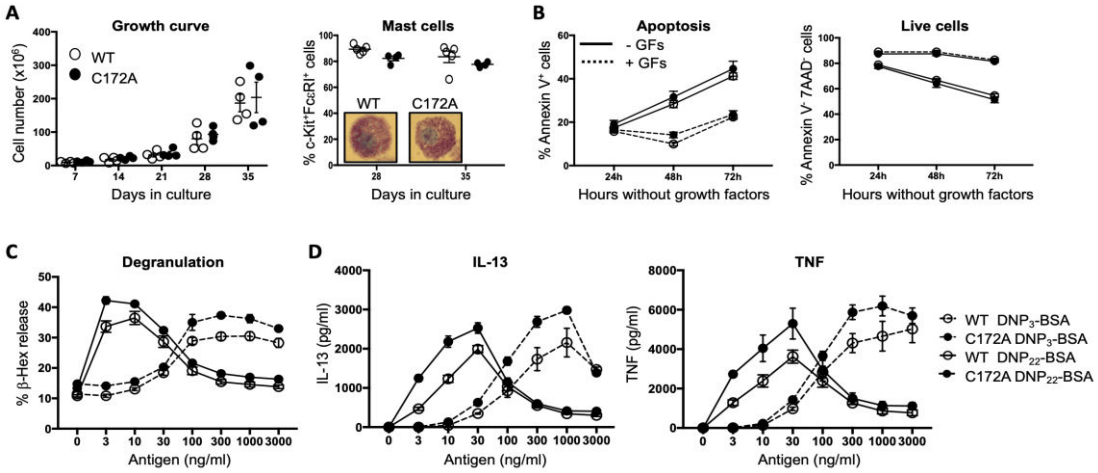

Figure S3: (Related to Fig. 2). Properties of BMMCs derived from HRF-C172A mice. (A) Development of c-Kit+ FcεRI+ BMMCs from HRF-C172A mice was compared with WT mice. Toluidine blue-stained BMMCs are included. (B) BMMCs from WT and HRF-C172A mice were subjected to growth factor deprivation for the indicated periods and stained for annexin V and 7AAD for flow cytometry. (C,D) BMMCs from WT and HRF-C172A mice sensitized overnight with anti-DNP IgE were stimulated with DNP3-BSA or DNP22-BSA for 30 min (for degranulation) or 16 h (for cytokines). Degranulation (C) and cytokine production/secretion (D) were quantified.

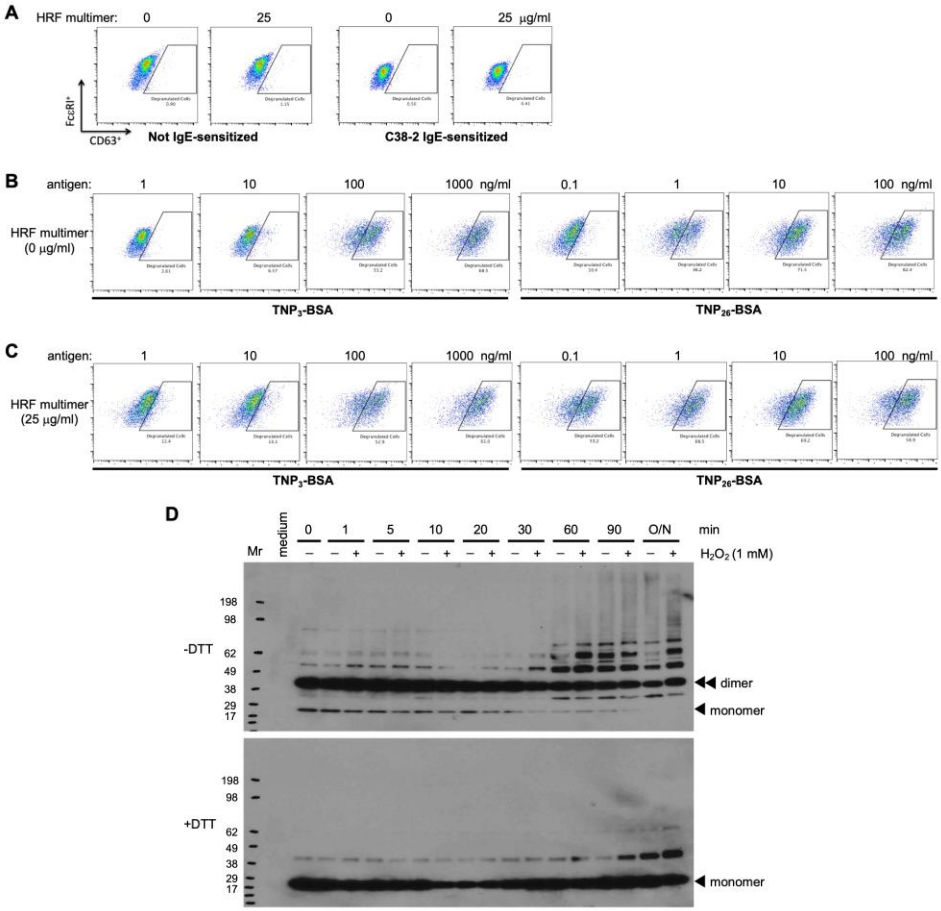

Figure S4: (Related to Fig. 3). Enhanced antigen-induced degranulation of mast cells by HRF multimers. (A-C) BMMCs were sensitized or not sensitized overnight with HRF-reactive anti-TNP IgE C38-2 (0.5 ◎g/ml), then incubated with 0 or 25 ◎g/ml of

mHRF multmers alone (A). (B,C) C38-2 IgE-sensitized cells were stimulated with the indicated concentrations of TNP3-BSA or TNP26-BSA in the presence or absence of HRF multimers (25 ⍵g/ml) for 30 min. Degranulation was assessed by flow cytometry of CD63+ Fc⍵RI+ cells. (D) Purified mHRF dimer (purity similar to the dimer shown in Fig. 2D) was incubated with or without 1 mM H2O2 in D10 medium for the indicated periods of time and analyzed by SDS-PAGE under non-reducing (-DTT) or reducing (+DTT) conditions, followed by western blotting for HRF.

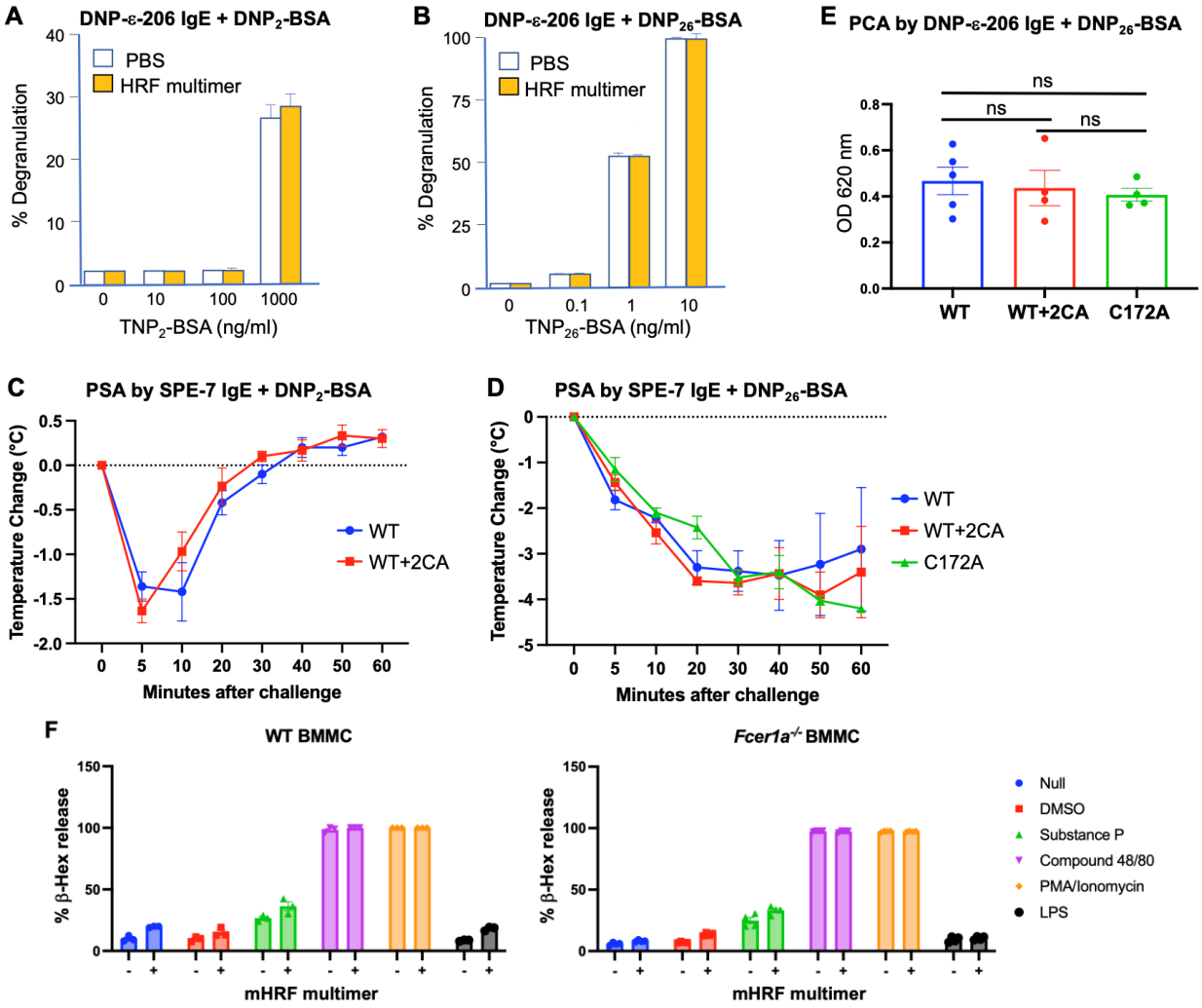

Figure S5: (Related to Figs. 3-5). Effects of HRF inhibitor and HRF-C172A mutation on *in-vitro* and *In-vivo* antigen-induced activation of mast cells sensitized with HRF-nonreactive IgE and effects of HRF multimers on non-Fc⍵RI stimulations in WT and Fcer1a-/- BMMCs. (A) BMMCs from WT mice were sensitized with HRF-nonreactive IgE (DNP-⍵-206 IgE or SPE-7 IgE) and stimulated by DNP2-BSA (A) or DNP26-BSA (B) with or without HRF multimers for 30 min. Surface expression of CD63 was measured by flow cytometry as a surrogate of degranulation. Data with SPE-7 IgE sensitization gave similar results with DNP-⍵-206 IgE sensitization (data not shown). (C,D) Mice were passively sensitized with anti-DNP IgE SPE-7. 24 h later, PSA was induced by antigen DNP2-BSA or DNP26-BSA with or without HRF inhibitor pretreatment in WT mice (C) or HRF-C172A mice (D). Body surface temperature was measured. (E) 24 h after passive sensitization by intradermal injection of DNP-⍵-206 IgE or PBS at the ear, PCA was induced by antigen DNP26-BSA (or PBS as a negative control) together with Evans' blue dye with or without HRF-2CA pretreatment in WT or HRF-C172A mice. Dye extravasation was quantified. ns, nonsignificant. (F) WT and Fcer1-/- BMMCs were stimulated with the indicated agents in the absence or presence of 25 ⍵g/ml of HRF multimers for 30 min. ⍵-hexosaminidase released from activated mast cells were measured. PMA, phorbol myristate acetate; LPS, lipopolysaccharide.

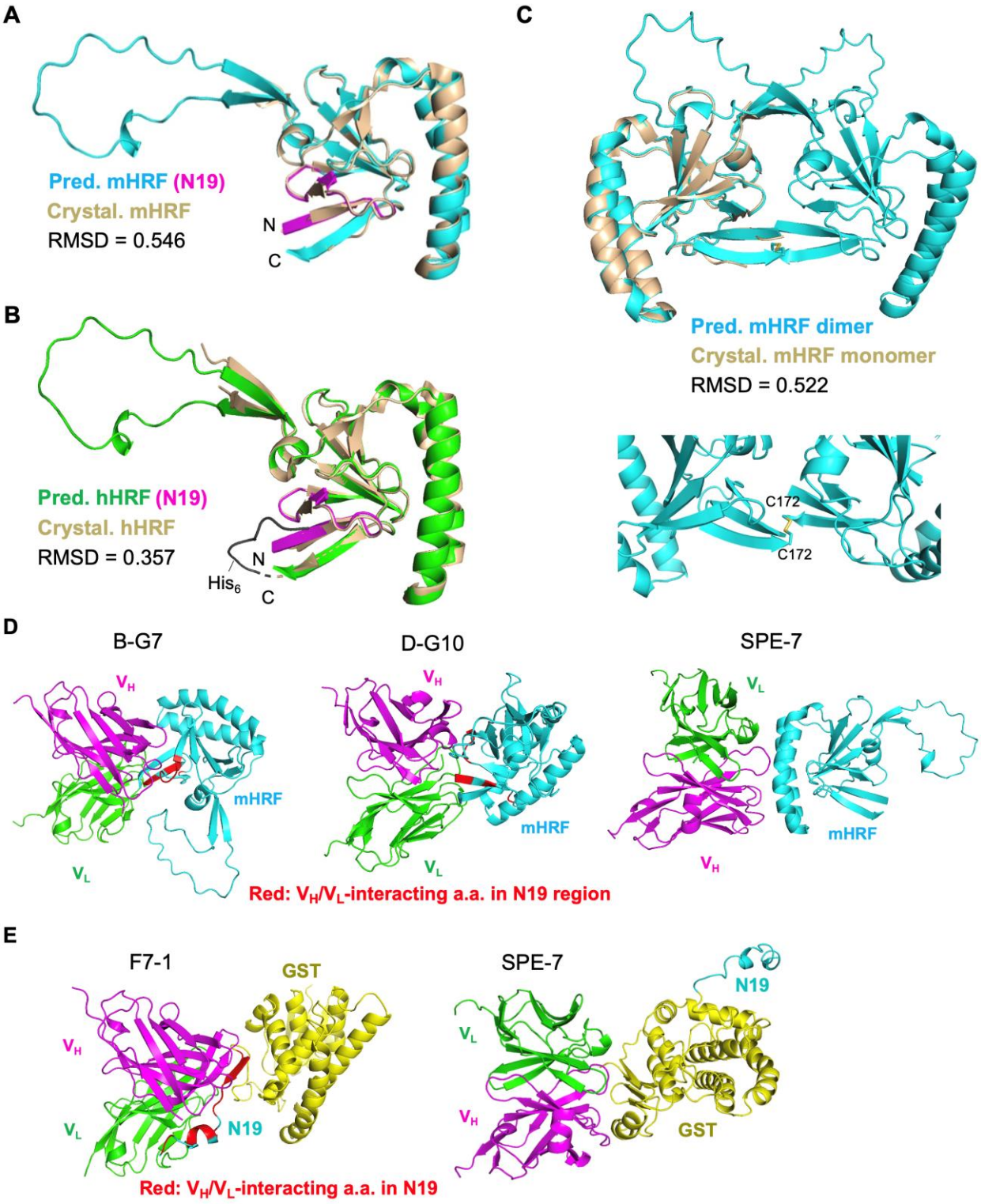
A
Pred. mHRF (N19)
Crystal. mHRF
RMSD = 0.546
N
C
B
Pred. hHRF (N19)
Crystal. hHRF
RMSD = 0.357
N
His6
C
C
Pred. mHRF dimer
Crystal. mHRF monomer
RMSD = 0.522
C172
C172
D
B-G7
D-G10
SPE-7
VH
VL
mHRF
Red: VH/VL-interacting a.a. in N19 region
E
F7-1
GST
VH
VL
N19
SPE-7
N19
VL
VH
GST
Red: VH/VL-interacting a.a. in N19

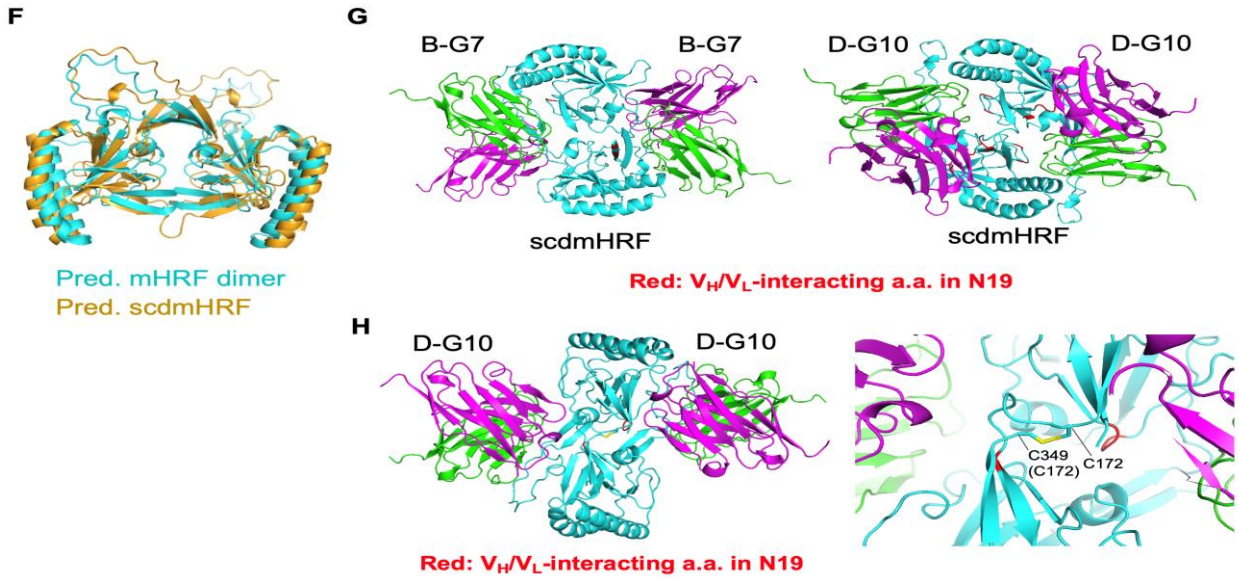

Figure S6: (Related to Figs. 2-7). Predicted structures of an HRF monomer and dimer and their complexes with HRF-reactive Ig molecules. (A,B) Alignments of predicted (Pred.) HRF monomers were made with the corresponding HRF monomers revealed by crystallography (Crystal.). Murine HRF (A) and human HRF (B). N- and C-termini are labeled. RMSD, root mean square deviation. Note that the crystalized hHRF has a His6 tag. (C) A predicted mHRF dimer was aligned with a predicted hHRF dimer (Upper panel) with a blowup to show the C172-C172 disulfide linkage. (D) Predicted interactions between a mHRF monomer and B-G7, D-G10 or SPE-7 (VH/VL)1 domains. Rank 1 models in Table S4 are shown. Interfacing amino acid (a.a.) residues in N19 portion are highlighted in red. (E) Predicted interactions between GST-N19 and F7-1 or SPE-7 (VH/VL)1 domains. Rank 1 models in Table S4 are shown. (F) A predicted structure of the imaginary molecule, single-chain mHRF dimer (scdmHRF) was aligned with that of a disulfide-linked mHRF dimer. (G) Predicted interactions between scdmHRF and B-G7 or D-G10 (VH/VL)2 domains are shown (Rank 2 and rank1 models, respectively). (H) A predicted complex structure of scdmHRF and D-G10 (VH/VL)2 domains (Rank 2) contained C172-C349 disulfide linkage (corresponding to C172 of the latter mHRF in scdmHRF).

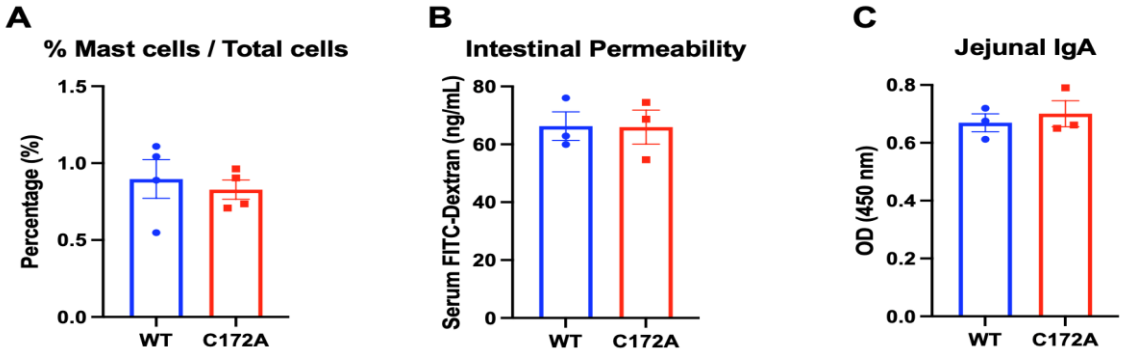

Figure S7: (Related to Fig. 6). Intestinal phenotypes of HRF-C172A mice. (A) Mast cell density in duodenum and jejunum, (B) intestinal permeability to 4 kDa FITC dextran and (C) jejunal IgA levels were compared between WT and HRF-C172A mice.